AIP | The Journal of Chemical Physics

Calculations of electric dipole moments and static dipole polarizabilities based on the two-component normalized elimination of the small component method

Terutaka Yoshizawa, Wenli Zou, and Dieter Cremer

Citation: The Journal of Chemical Physics **145**, 184104 (2016); doi: 10.1063/1.4964765
View online: http://dx.doi.org/10.1063/1.4964765
View Table of Contents: http://scitation.aip.org/content/aip/journal/jcp/145/18?ver=pdfcov
Published by the AIP Publishing

THE JOURNAL OF CHEMICAL PHYSICS **145**, 184104 (2016)

Calculations of electric dipole moments and static dipole polarizabilities based on the two-component normalized elimination of the small component method

Terutaka Yoshizawa, Wenli Zou, and Dieter Cremer[a)]
Department of Chemistry, Southern Methodist University, 3215 Daniel Ave., Dallas, Texas 75275-0314, USA

(Received 27 July 2016; accepted 29 September 2016; published online 8 November 2016)

The analytical energy gradient and Hessian of the two-component Normalized Elimination of the Small Component (2c-NESC) method with regard to the components of the electric field are derived and used to calculate spin-orbit coupling (SOC) corrected dipole moments and dipole polarizabilities of molecules, which contain elements with high atomic number. Calculated 2c-NESC dipole moments and isotropic polarizabilities agree well with the corresponding four-component-Dirac Hartree–Fock or density functional theory values. SOC corrections for the electrical properties are in general small, but become relevant for the accurate prediction of these properties when the molecules in question contain sixth and/or seventh period elements (e.g., the SO effect for At_2 is about 10% of the 2c-NESC polarizability). The 2c-NESC changes in the electric molecular properties are rationalized in terms of spin-orbit splitting and SOC-induced mixing of frontier orbitals with the same $j = l + s$ quantum numbers. *Published by AIP Publishing.* [http://dx.doi.org/10.1063/1.4964765]

I. INTRODUCTION

This work is part of a larger project focused on implementing first-order and second-order response properties via analytical energy derivatives for a Dirac-exact one-component (1c) and two-component (2c) methods. Exact 1c-relativistic one-electron Hamiltonians can be considered to accurately and reliably include scalar relativistic effects whereas exact 2c-methods also include spin-orbit coupling (SOC) effects into the quantum chemical description.[1,2] Solution of the Dirac equation leads to four-component (4c) wavefunctions, which include the description of both electron and positron spins.[3,4] The normalized elimination of the small component (NESC) method of Dyall[5] separates the calculation of the electron and positron states via the elimination of the small component of the relativistic wave function. Dyall's work in the 1990s initiated the development of Dirac-exact 1c- and 2c-relativistic methods and their use in chemistry.

In previous work, we have developed a new algorithm for the execution of NESC calculations[6] and the analytical first derivatives of 1c-NESC to routinely calculate first-order response properties such as molecular geometries,[7] electric dipole moments,[8] EPR hyperfine structure constants,[9] contact densities for the calculation of Mössbauer isomer shifts,[10] and electric field gradients for nuclear quadrupole coupling constants.[11] In an extension of this work, we also developed algorithms to calculate second-order response properties such as vibrational frequencies,[8,12] static electric polarizabilities,[8] and infrared intensities.[8] These methods were applied to pending chemical problems.[8,13–15]

Recently, we began to install first- and second-order response properties for 2c-NESC to study the effects of SOC on molecular properties.[1,2,16–22] For this purpose, we combined the 2c-NESC method and general Hartree Fock (GHF) or, alternatively, general density functional theory (GDFT) to determine a suitable reference wave function.[23] We succeeded in developing the analytical energy gradient to carry out geometry optimizations at the 2c-NESC level of theory.[24] In the current work, we use the energy gradient algorithm to reliably determine electrical properties such as the molecular dipole moment. In addition, we develop second derivatives of the 2c-NESC electronic energy to calculate second-order electrical response properties such as the static electric dipole polarizability. This implies the development of a suitable coupled perturbed GHF (CPGHF)[25] or coupled perturbed Kohn-Sham (CPGKS) approach,[26–29] which are both presented in this work. The CPGHF and CPGKS methods have already been used in 2c-relativistic property calculations, but to the best of our knowledge the CPGKS approach for the non-collinear exchange-correlation (XC) potential[30–32] or the long-range corrected (LC) exchange functional[33,34] have so far not been developed. Apart from this, we install CPGHF and CPGKS into 2c-NESC to exploit the compact and efficient programming of NESC response properties in terms of products of traces of matrices[35,36] to provide the possibility of a rapid calculation of first and second order 2c-NESC response properties. Hence, we consider the presentation of the CPGHF/CPGKS equations of 2c-NESC as the basis for our future work on vibrational frequencies, infrared intensities, and other 2nd-order properties of 2c-NESC.

This work is focused on the development of 2c-NESC for its routine calculation of response properties. Apart from

[a)]Author to whom correspondence should be addressed. Electronic mail: dieter.cremer@gmail.com

this, we want to investigate SOC effects on electric properties. Generally, they become small when the property in question depends just on the distribution of the valence electrons. For example, in the case of the polarizability, the distortion of the molecular electronic structure exposed to an electric field changes through a mixing of outer valence and virtual orbitals. Since the SOC is smallest for the outer valence orbitals, a large SOC effect cannot be expected. For the dipole moment, the SOC effect should be larger as in this case the inner valence orbitals are more involved.

The results of this work are presented in three sections. In Section II, we will describe the basic theory for obtaining the 2c-NESC/GHF and 2c-NESC/GDFT gradient and Hessian calculated with regard to the components of an electric field. In Section III, the implementation of the 2c-NESC Hessian and computational details of its application are described and in Section IV, 2c-NESC dipole moments and polarizabilities are analyzed. Section V summarizes the conclusions of the current SOC investigation.

II. THEORY

The renormalized one-electron NESC Hamiltonian is given by

$$\mathbf{H}_{1e} = \mathbf{G}^{\dagger}\tilde{\mathbf{L}}\mathbf{G}, \tag{1}$$

where the renormalization matrix $\mathbf{G}$[37] is given by

$$\mathbf{G} = \mathbf{S}^{-1/2}\left(\mathbf{S}^{-1/2}\tilde{\mathbf{S}}\mathbf{S}^{-1/2}\right)^{-1/2}\mathbf{S}^{1/2}, \tag{2}$$

$$\tilde{\mathbf{S}} = \mathbf{S} + \frac{1}{2mc^2}\left(\mathbf{U}^{\dagger}\mathbf{T}\mathbf{U}\right), \tag{3}$$

and the NESC Hamiltonian matrix $\tilde{\mathbf{L}}$ is defined by[5,6,38–40]

$$\tilde{\mathbf{L}} = \mathbf{T}\mathbf{U} + \mathbf{U}^{\dagger}\mathbf{T} - \mathbf{U}^{\dagger}\left(\mathbf{T}-\mathbf{W}\right)\mathbf{U} + \mathbf{V}. \tag{4}$$

Symbols $\mathbf{T}$, $\mathbf{V}$, and $\mathbf{S}$ correspond to the kinetic energy, potential energy, and overlap matrix in the 2c-form (dimension 2M × 2M: M: number of basis functions) whereas $\mathbf{U}$ is the matrix which connects the large component $\mathbf{A}_+$ and the pseudolarge component $\mathbf{B}_+$ via $\mathbf{B}_+ = \mathbf{U}\mathbf{A}_+$.[5,6] Matrix $\mathbf{W}$ is associated with the operator $(\boldsymbol{\sigma}\cdot\mathbf{p})V(\mathbf{r})(\boldsymbol{\sigma}\cdot\mathbf{p})/(4m^2c^2)$, where $\mathbf{p}$ is the momentum operator, $\boldsymbol{\sigma}$ is the vector of the three Pauli spin matrices, and $\mathbf{r}$ is the position vector of the electron.

One of the referees has pointed out that a more appropriate term for a method based on Eq. (1) is X2C[41] (or NESC/X2C) as it leads from the Dirac picture to the Schrödinger picture.

The first derivative of the renormalized NESC Hamiltonian with regard to the perturbation λ is given by[7]

$$\frac{\partial \mathbf{H}_{1e}}{\partial\lambda} = \mathbf{G}^{\dagger}\frac{\partial\tilde{\mathbf{L}}}{\partial\lambda}\mathbf{G} + \frac{\partial\mathbf{G}^{\dagger}}{\partial\lambda}\tilde{\mathbf{L}}\mathbf{G} + \mathbf{G}^{\dagger}\tilde{\mathbf{L}}\frac{\partial\mathbf{G}}{\partial\lambda}. \tag{5}$$

First- and second-order properties are calculated utilizing the following:

$$tr\mathbf{P}\frac{\partial \mathbf{H}_{1e}}{\partial\lambda} = tr\tilde{\mathbf{P}}\frac{\partial\tilde{\mathbf{L}}}{\partial\lambda} + tr\mathbf{D}\frac{\partial\mathbf{G}^{\dagger}}{\partial\lambda} + tr\mathbf{D}^{\dagger}\frac{\partial\mathbf{G}}{\partial\lambda}, \tag{6}$$

where $\mathbf{P}$ is a general density matrix (i.e., a zeroth-order density matrix for first-order properties or a first-order density matrix for second-order properties), $\tilde{\mathbf{P}} = \mathbf{G}\mathbf{P}\mathbf{G}^{\dagger}$, and $\mathbf{D} = \tilde{\mathbf{L}}\mathbf{G}\mathbf{P}$. The derivative of $\tilde{\mathbf{L}}$ in Eq. (6) is written as

$$\begin{aligned}\frac{\partial\tilde{\mathbf{L}}}{\partial\lambda} &= \mathbf{U}^{\dagger}\frac{\partial\mathbf{T}}{\partial\lambda} + \frac{\partial\mathbf{T}}{\partial\lambda}\mathbf{U} - \mathbf{U}^{\dagger}\frac{\partial\mathbf{T}}{\partial\lambda}\mathbf{U} + \mathbf{U}^{\dagger}\frac{\partial\mathbf{W}}{\partial\lambda}\mathbf{U} + \frac{\partial\mathbf{V}}{\partial\lambda}\\ &\quad + \frac{\partial\mathbf{U}^{\dagger}}{\partial\lambda}\left[\mathbf{T}-\left(\mathbf{T}-\mathbf{W}\right)\mathbf{U}\right] + \left[\mathbf{T}-\mathbf{U}^{\dagger}\left(\mathbf{T}-\mathbf{W}\right)\right]\frac{\partial\mathbf{U}}{\partial\lambda},\end{aligned} \tag{7}$$

and the second and third terms of Eq. (6) are given by

$$\begin{aligned}tr\mathbf{D}\frac{\partial\mathbf{G}^{\dagger}}{\partial\lambda} + tr\mathbf{D}^{\dagger}\frac{\partial\mathbf{G}}{\partial\lambda} &= tr\mathbf{P}_{GS}\frac{\partial\mathbf{S}}{\partial\lambda} + tr\mathbf{P}_{GT}\frac{\partial\mathbf{T}}{\partial\lambda}\\ &\quad + tr\left(\mathbf{P}^{\dagger}_{GU}\frac{\partial\mathbf{U}^{\dagger}}{\partial\lambda} + \mathbf{P}_{GU}\frac{\partial\mathbf{U}}{\partial\lambda}\right),\end{aligned} \tag{8}$$

where the detailed definitions of $\mathbf{P}_{GS}$, $\mathbf{P}_{GT}$, and $\mathbf{P}_{GU}$ are given in Eq. (20) of Ref. 24. There, the three matrices are calculated by using the eigenvalues and eigenvectors of $\mathbf{G}$. By inserting Eqs. (7) and (8) into Eq. (6), $tr\mathbf{P}(\partial\mathbf{H}_{1e}/\partial\lambda)$ of Eq. (6) becomes

$$\begin{aligned}tr\mathbf{P}\frac{\partial\mathbf{H}_{1e}}{\partial\lambda} &= tr\mathbf{P}_{GS}\frac{\partial\mathbf{S}}{\partial\lambda}\\ &\quad + tr\left(\mathbf{U}\tilde{\mathbf{P}} + \tilde{\mathbf{P}}\mathbf{U}^{\dagger} - \mathbf{U}\tilde{\mathbf{P}}\mathbf{U}^{\dagger} + \mathbf{P}_{GT}\right)\frac{\partial\mathbf{T}}{\partial\lambda}\\ &\quad + tr\tilde{\mathbf{P}}\frac{\partial\mathbf{V}}{\partial\lambda} + tr\left(\mathbf{U}\tilde{\mathbf{P}}\mathbf{U}^{\dagger}\right)\frac{\partial\mathbf{W}}{\partial\lambda}\\ &\quad + tr\left(\mathbf{P}^{\dagger}_{U}\frac{\partial\mathbf{U}^{\dagger}}{\partial\lambda} + \mathbf{P}_{U}\frac{\partial\mathbf{U}}{\partial\lambda}\right),\end{aligned} \tag{9}$$

where $\mathbf{P}_U = \tilde{\mathbf{P}}\left[\mathbf{T}-\mathbf{U}^{\dagger}(\mathbf{T}-\mathbf{W})\right] + \mathbf{P}_{GU}$. The last term of Eq. (9) is obtained by

$$\begin{aligned}tr\mathbf{P}_U\frac{\partial\mathbf{U}}{\partial\lambda} &= tr\mathbf{P}_{US}\frac{\partial\mathbf{S}}{\partial\lambda} + tr\mathbf{P}_{UT}\frac{\partial\mathbf{T}}{\partial\lambda}\\ &\quad + tr\mathbf{P}_{UV}\frac{\partial\mathbf{V}}{\partial\lambda} + tr\mathbf{P}_{UW}\frac{\partial\mathbf{W}}{\partial\lambda},\end{aligned} \tag{10}$$

where the matrices $\mathbf{P}_{US}$, $\mathbf{P}_{UT}$, $\mathbf{P}_{UV}$, and $\mathbf{P}_{UW}$ are calculated by using the eigenvalues and eigenvectors of the one-electron Dirac Hamiltonian. Detailed formulas are given in Eqs. (B14)–(B17) of Ref. 12. Insertion of Eq. (10) into Eq. (9) leads to Eq. (11),

$$tr\mathbf{P}\frac{\partial\mathbf{H}_{1e}}{\partial\lambda} = tr\mathbf{P}_S\frac{\partial\mathbf{S}}{\partial\lambda} + tr\mathbf{P}_T\frac{\partial\mathbf{T}}{\partial\lambda} + tr\mathbf{P}_V\frac{\partial\mathbf{V}}{\partial\lambda} + tr\mathbf{P}_W\frac{\partial\mathbf{W}}{\partial\lambda}, \tag{11}$$

where $\mathbf{P}_S = \mathbf{P}_{GS} + \mathbf{P}_{US} + \mathbf{P}^{\dagger}_{US}$, $\mathbf{P}_T = \mathbf{U}\tilde{\mathbf{P}} + \tilde{\mathbf{P}}\mathbf{U}^{\dagger} - \mathbf{U}\tilde{\mathbf{P}}\mathbf{U}^{\dagger} + \mathbf{P}_{GT} + \mathbf{P}_{UT} + \mathbf{P}^{\dagger}_{UT}$, $\mathbf{P}_V = \tilde{\mathbf{P}} + \mathbf{P}_{UV} + \mathbf{P}^{\dagger}_{UV}$, and $\mathbf{P}_W = \mathbf{U}\tilde{\mathbf{P}}\mathbf{U}^{\dagger} + \mathbf{P}_{UW} + \mathbf{P}^{\dagger}_{UW}$.[24]

A. Calculation of the dipole moment at 2c-NESC/GHF

By considering the interaction between an electronic system and an external electric field $\mathbf{F}$ as perturbation, the perturbation parameter λ in Eq. (11) corresponds to the components F_t $(t = x, y, z)$ of the electric field and the potential energy V has to be rewritten as

$$V(\mathbf{r}) = V_{nuc}(\mathbf{F}=\mathbf{0}) + \mathbf{F}\cdot\mathbf{r}. \tag{12}$$

Then, the dipole moment $\boldsymbol{\mu}$ is given by

$$\mu_t = -tr\left[\mathbf{P}\frac{\partial \mathbf{H}_{1e}}{\partial F_t}\right]_{\mathbf{F=0}} = -tr\left[\mathbf{P}_V\frac{\partial \mathbf{V}}{\partial F_t} + \mathbf{P}_W\frac{\partial \mathbf{W}}{\partial F_t}\right]_{\mathbf{F=0}}. \quad (13)$$

Here, $\mathbf{P}$ is the zeroth-order density matrix at the 2c level (see Eq. (19)). The derivative of the potential energy with regard to the electric field is calculated utilizing the non-relativistic dipole integrals

$$\left.\frac{\partial \mathbf{V}}{\partial F_t}\right|_{\mathbf{F=0}} = \begin{pmatrix} \mathbf{M}_t & \mathbf{0} \\ \mathbf{0} & \mathbf{M}_t \end{pmatrix}, \quad (14)$$

where $M_{\mu\nu,t} = (\mu|r_t|\nu)$ (μ, ν: basis function indices). The corresponding derivative of the $\mathbf{W}$ matrix has to consider real and imaginary parts,

$$\left.\frac{\partial \mathbf{W}}{\partial F_t}\right|_{\mathbf{F=0}} = \begin{pmatrix} \tilde{\mathbf{W}}_{sf} + i\tilde{\mathbf{W}}_z & i\tilde{\mathbf{W}}_x + \tilde{\mathbf{W}}_y \\ i\tilde{\mathbf{W}}_x - \tilde{\mathbf{W}}_y & \tilde{\mathbf{W}}_{sf} - i\tilde{\mathbf{W}}_z \end{pmatrix}. \quad (15)$$

Index *sf* denotes the *spin-free* part and $i = \sqrt{-1}$. The elements of $\tilde{\mathbf{W}}$ are defined by

$$\tilde{\mathbf{W}}_{\mu\nu,sf} = \frac{1}{4m^2c^2}(\mu|\mathbf{p}r_t\mathbf{p}|\nu), \quad (16)$$

$$\tilde{\mathbf{W}}_{\mu\nu,u} = \frac{1}{4m^2c^2}(\mu|(\mathbf{p}r_t \times \mathbf{p})_u|\nu), \quad (17)$$

for $u = x, y, z$.

B. Calculation of the dipole polarizability at 2c-NESC/GHF

The elements of the polarizability tensor $\boldsymbol{\alpha}$ are given by[8,42]

$$\alpha_{tu} = -\left.\frac{\partial^2 E}{\partial F_t \partial F_u}\right|_{\mathbf{F=0}} = -tr\left[\mathbf{P}_t^{(1)}\left(\mathbf{G}^\dagger\left(\frac{\partial \mathbf{V}}{\partial F_u} + \mathbf{U}^\dagger\frac{\partial \mathbf{W}}{\partial F_u}\mathbf{U}\right)\mathbf{G}\right)\right], \quad (18)$$

where $t, u = x, y, z$. The term $\mathbf{U}^\dagger(\partial\mathbf{W}/\partial F_u)\mathbf{U}$ makes only a very small contribution to the dipole polarizability ($<10^{-3}$ a.u.) as was expected by Zou and co-workers.[8,42] Nevertheless, we have included the second term in this work.

In Eq. (18), E is the total electronic energy and $\mathbf{P}_t^{(1)}$ is the first-order density matrix (i.e., $\partial\mathbf{P}/\partial F_t$) which is obtained by solving the CPGHF problem. The first-order density matrix $\mathbf{P}_t^{(1)}$ is defined by

$$\mathbf{P}_t^{(1)} = \begin{pmatrix} \mathbf{P}_t^{(1)\alpha\alpha} & \mathbf{P}_t^{(1)\alpha\beta} \\ \mathbf{P}_t^{(1)\beta\alpha} & \mathbf{P}_t^{(1)\beta\beta} \end{pmatrix}, \quad (19)$$

where its elements are given by

$$P_{\sigma\lambda,t}^{(1)\alpha\alpha} = \sum_j^{occ}\left(C_{\sigma j,t}^{(1)\alpha *}C_{\lambda j}^{\alpha} + C_{\sigma j}^{\alpha *}C_{\lambda j,t}^{(1)\alpha}\right), \quad (20)$$

$$P_{\sigma\lambda,t}^{(1)\beta\beta} = \sum_j^{occ}\left(C_{\sigma j,t}^{(1)\beta *}C_{\lambda j}^{\beta} + C_{\sigma j}^{\beta *}C_{\lambda j,t}^{(1)\beta}\right), \quad (21)$$

$$P_{\sigma\lambda,t}^{(1)\beta\alpha} = \sum_j^{occ}\left(C_{\sigma j,t}^{(1)\beta *}C_{\lambda j}^{\alpha} + C_{\sigma j}^{\beta *}C_{\lambda j,t}^{(1)\alpha}\right), \quad (22)$$

$$P_{\sigma\lambda,t}^{(1)\alpha\beta} = \sum_j^{occ}\left(C_{\sigma j,t}^{(1)\alpha *}C_{\lambda j}^{\beta} + C_{\sigma j}^{\alpha *}C_{\lambda j,t}^{(1)\beta}\right). \quad (23)$$

The molecular spinor coefficients $\mathbf{C}^\alpha$ and $\mathbf{C}^\beta$ are obtained by solving the GHF equation

$$\begin{pmatrix} \mathbf{F}^{\alpha\alpha} & \mathbf{F}^{\alpha\beta} \\ \mathbf{F}^{\beta\alpha} & \mathbf{F}^{\beta\beta} \end{pmatrix}\begin{pmatrix} \mathbf{C}^\alpha \\ \mathbf{C}^\beta \end{pmatrix} = \begin{pmatrix} \mathbf{S} & \mathbf{0} \\ \mathbf{0} & \mathbf{S} \end{pmatrix}\begin{pmatrix} \mathbf{C}^\alpha \\ \mathbf{C}^\beta \end{pmatrix}\boldsymbol{\epsilon}. \quad (24)$$

The components of the Fock matrix for the 2c-NESC method are given by

$$F_{\mu\nu}^{\alpha\alpha} = H_{\mu\nu}^{NESC,\alpha\alpha} + \sum_{\sigma,\lambda}\left[\left(P_{\sigma\lambda}^{\alpha\alpha} + P_{\sigma\lambda}^{\beta\beta}\right)(\mu\nu|\sigma\lambda) - P_{\lambda\sigma}^{\alpha\alpha *}(\mu\lambda|\sigma\nu)\right], \quad (25)$$

$$F_{\mu\nu}^{\beta\beta} = H_{\mu\nu}^{NESC,\beta\beta} + \sum_{\sigma,\lambda}\left[\left(P_{\sigma\lambda}^{\alpha\alpha} + P_{\sigma\lambda}^{\beta\beta}\right)(\mu\nu|\sigma\lambda) - P_{\lambda\sigma}^{\beta\beta *}(\mu\lambda|\sigma\nu)\right], \quad (26)$$

$$F_{\mu\nu}^{\beta\alpha} = H_{\mu\nu}^{NESC,\beta\alpha} - \sum_{\sigma,\lambda}P_{\lambda\sigma}^{\beta\alpha *}(\mu\lambda|\sigma\nu), \quad (27)$$

$$F_{\mu\nu}^{\alpha\beta} = H_{\mu\nu}^{NESC,\alpha\beta} - \sum_{\sigma,\lambda}P_{\lambda\sigma}^{\alpha\beta *}(\mu\lambda|\sigma\nu), \quad (28)$$

and the two-electron integrals are defined in the usual way. $\mathbf{H}^{NESC,\omega\omega'}$ ($\omega,\omega' = \alpha,\beta$) denotes the $\omega\omega'$ component of the renormalized one-electron NESC Hamiltonian $\mathbf{G}^\dagger\tilde{\mathbf{L}}\mathbf{G}$ and the zeroth-order density matrix $\mathbf{P}^{\omega\omega'}$ is given by $P_{\sigma\lambda}^{\omega\omega'} = \Sigma_i C_{\sigma i}^{\omega *}C_{\lambda i}^{\omega'}$.

In Eqs. (20)-(23), the first-order molecular spinor coefficients $\mathbf{C}^{(1)\alpha}$ and $\mathbf{C}^{(1)\beta}$ are obtained with the help of the mixing coefficient matrix $\mathbf{Y}^{(1)}$, which is a 2M × 2M matrix and includes $\alpha - \beta$ spin rotations:[25]

$$C_{\lambda j,t}^{(1)\alpha} = \sum_p^{MO}C_{\lambda p}^{\alpha}Y_{pj,t}^{(1)}, \quad (29)$$

$$C_{\lambda j,t}^{(1)\beta} = \sum_p^{MO}C_{\lambda p}^{\beta}Y_{pj,t}^{(1)}. \quad (30)$$

Here, we use the non-canonical solutions for the diagonal blocks of the $\mathbf{Y}^{(1)}$ matrix:

$$Y_{ij,t}^{(1)} = Y_{ji,t}^{(1)*} \qquad (i,j \in occ). \quad (31)$$

Thus, from Eq. (31) and the form of the orthonormality condition

$$\begin{pmatrix} \mathbf{C}^{(1)\alpha\dagger} & \mathbf{C}^{(1)\beta\dagger} \end{pmatrix}\begin{pmatrix} \mathbf{S} & \mathbf{0} \\ \mathbf{0} & \mathbf{S} \end{pmatrix}\begin{pmatrix} \mathbf{C}^\alpha \\ \mathbf{C}^\beta \end{pmatrix} + \begin{pmatrix} \mathbf{C}^{\alpha\dagger} & \mathbf{C}^{\beta\dagger} \end{pmatrix}\begin{pmatrix} \mathbf{S} & \mathbf{0} \\ \mathbf{0} & \mathbf{S} \end{pmatrix}\begin{pmatrix} \mathbf{C}^{(1)\alpha} \\ \mathbf{C}^{(1)\beta} \end{pmatrix} = \mathbf{0}, \quad (32)$$

one obtains

$$Y_{ij,t}^{(1)} = 0 \qquad (i,j \in occ). \quad (33)$$

The occupied-virtual part of the mixing coefficient matrix $Y^{(1)}_{bj,t}$ ($j \in occ,\ b \in vir$) is determined by the derivative of the GHF equation

$$\begin{pmatrix} \mathbf{F}^{\alpha\alpha} & \mathbf{F}^{\alpha\beta} \\ \mathbf{F}^{\beta\alpha} & \mathbf{F}^{\beta\beta} \end{pmatrix}\begin{pmatrix} \mathbf{C}^{(1)\alpha}_t \\ \mathbf{C}^{(1)\beta}_t \end{pmatrix} + \begin{pmatrix} \mathbf{F}^{(1)\alpha\alpha}_t & \mathbf{F}^{(1)\alpha\beta}_t \\ \mathbf{F}^{(1)\beta\alpha}_t & \mathbf{F}^{(1)\beta\beta}_t \end{pmatrix}\begin{pmatrix} \mathbf{C}^{\alpha} \\ \mathbf{C}^{\beta} \end{pmatrix} = \begin{pmatrix} \mathbf{S} & \mathbf{0} \\ \mathbf{0} & \mathbf{S} \end{pmatrix}\begin{pmatrix} \mathbf{C}^{(1)\alpha}_t \\ \mathbf{C}^{(1)\beta}_t \end{pmatrix}\boldsymbol{\epsilon} + \begin{pmatrix} \mathbf{S} & \mathbf{0} \\ \mathbf{0} & \mathbf{S} \end{pmatrix}\begin{pmatrix} \mathbf{C}^{\alpha} \\ \mathbf{C}^{\beta} \end{pmatrix}\boldsymbol{\epsilon}^{(1)}_t. \tag{34}$$

By setting $\epsilon^{(1)}_{ia,t} = \epsilon^{(1)}_{ai,t} = 0$ ($i \in occ,\ a \in vir$), the matrix $Y^{(1)}_{bj,t}$ can be written according to

$$Y^{(1)}_{bj,t} = \frac{1}{\epsilon_j - \epsilon_b}\sum_{\mu,\nu}(C^{\alpha*}_{\mu b}F^{(1)\alpha\alpha}_{\mu\nu,t}C^{\alpha}_{\nu j} + C^{\alpha*}_{\mu b}F^{(1)\alpha\beta}_{\mu\nu,t}C^{\beta}_{\nu j} + C^{\beta*}_{\mu b}F^{(1)\beta\alpha}_{\mu\nu,t}C^{\alpha}_{\nu j} + C^{\beta*}_{\mu b}F^{(1)\beta\beta}_{\mu\nu,t}C^{\beta}_{\nu j}). \tag{35}$$

In Eq. (35), the elements of the first-order Fock matrix are defined by

$$F^{(1)\alpha\alpha}_{\mu\nu,t} = H^{(1)NESC,\alpha\alpha}_{\mu\nu,t} + \sum_{\sigma,\lambda}\left[\left(P^{(1)\alpha\alpha}_{\sigma\lambda,t} + P^{(1)\beta\beta}_{\sigma\lambda,t}\right)(\mu\nu|\sigma\lambda) - P^{(1)\alpha\alpha*}_{\lambda\sigma,t}(\mu\lambda|\sigma\nu)\right], \tag{36}$$

$$F^{(1)\beta\beta}_{\mu\nu,t} = H^{(1)NESC,\beta\beta}_{\mu\nu,t} + \sum_{\sigma,\lambda}\left[\left(P^{(1)\alpha\alpha}_{\sigma\lambda,t} + P^{(1)\beta\beta}_{\sigma\lambda,t}\right)(\mu\nu|\sigma\lambda) - P^{(1)\beta\beta*}_{\lambda\sigma,t}(\mu\lambda|\sigma\nu)\right], \tag{37}$$

$$F^{(1)\beta\alpha}_{\mu\nu,t} = H^{(1)NESC,\beta\alpha}_{\mu\nu,t} - \sum_{\sigma,\lambda}P^{(1)\beta\alpha*}_{\lambda\sigma,t}(\mu\lambda|\sigma\nu), \tag{38}$$

$$F^{(1)\alpha\beta}_{\mu\nu,t} = H^{(1)NESC,\alpha\beta}_{\mu\nu,t} - \sum_{\sigma,\lambda}P^{(1)\alpha\beta*}_{\lambda\sigma,t}(\mu\lambda|\sigma\nu). \tag{39}$$

Here, the following relationship is used:

$$\begin{pmatrix} \mathbf{H}^{(1)NESC,\alpha\alpha}_t & \mathbf{H}^{(1)NESC,\alpha\beta}_t \\ \mathbf{H}^{(1)NESC,\beta\alpha}_t & \mathbf{H}^{(1)NESC,\beta\beta}_t. \end{pmatrix} = \mathbf{G}^{\dagger}\left(\frac{\partial \mathbf{V}}{\partial F_t} + \mathbf{U}^{\dagger}\frac{\partial \mathbf{W}}{\partial F_t}\mathbf{U}\right)\mathbf{G}. \tag{40}$$

Combining the CPGHF method with the direct inversion in the iterative subspace (DIIS) method,[43,44] we iteratively obtain the first-order density matrix $\mathbf{P}^{(1)}_t$ based on Eqs. (19), (29), (30), (35), and (36)-(39).

C. Calculation of the dipole polarizability at 2c-NESC/GKS

To extend the Fock matrix for GHF to the GKS method, we replace the GHF exact exchange term by the exchange-correlation (XC) term in Eqs. (25)-(28),

$$\begin{pmatrix} \mathbf{K}^{\alpha\alpha}_{EX} & \mathbf{K}^{\alpha\beta}_{EX} \\ \mathbf{K}^{\beta\alpha}_{EX} & \mathbf{K}^{\beta\beta}_{EX} \end{pmatrix} \rightarrow \begin{pmatrix} \mathbf{K}^{\alpha\alpha}_{XC} & \mathbf{K}^{\alpha\beta}_{XC} \\ \mathbf{K}^{\beta\alpha}_{XC} & \mathbf{K}^{\beta\beta}_{XC} \end{pmatrix}. \tag{41}$$

In the pure-, hybrid-, or LC (long-range corrected)-DFT approach the elements of the GKS matrix are written as

$$F^{\alpha\alpha}_{\mu\nu} = H^{NESC,\alpha\alpha}_{\mu\nu} + \sum_{\sigma,\lambda}\left(P^{\alpha\alpha}_{\sigma\lambda} + P^{\beta\beta}_{\sigma\lambda}\right)(\mu\nu|\sigma\lambda) - \sum_{\sigma,\lambda}P^{\alpha\alpha*}_{\lambda\sigma}\left[a\,(\mu\lambda|\sigma\nu) + b(\mu\lambda|\sigma\nu)^{LR}\right] + bV^{\alpha\alpha}_{\mu\nu,XC}, \tag{42}$$

$$F^{\beta\beta}_{\mu\nu} = H^{NESC,\beta\beta}_{\mu\nu} + \sum_{\sigma,\lambda}\left(P^{\alpha\alpha}_{\sigma\lambda} + P^{\beta\beta}_{\sigma\lambda}\right)(\mu\nu|\sigma\lambda) - \sum_{\sigma,\lambda}P^{\beta\beta*}_{\lambda\sigma}\left[a\,(\mu\lambda|\sigma\nu) + b(\mu\lambda|\sigma\nu)^{LR}\right] + bV^{\beta\beta}_{\mu\nu,XC}, \tag{43}$$

$$F^{\beta\alpha}_{\mu\nu} = H^{NESC,\beta\alpha}_{\mu\nu} - \sum_{\sigma,\lambda}P^{\beta\alpha*}_{\lambda\sigma}\left[a\,(\mu\lambda|\sigma\nu) + b(\mu\lambda|\sigma\nu)^{LR}\right] + bV^{\beta\alpha}_{\mu\nu,XC}, \tag{44}$$

$$F^{\alpha\beta}_{\mu\nu} = H^{NESC,\alpha\beta}_{\mu\nu} - \sum_{\sigma,\lambda}P^{\alpha\beta*}_{\lambda\sigma}\left[a\,(\mu\lambda|\sigma\nu) + b(\mu\lambda|\sigma\nu)^{LR}\right] + bV^{\alpha\beta}_{\mu\nu,XC}, \tag{45}$$

where the parameter a gives the fraction of the GHF exchange term and parameter b the fraction of the long-range (LR) GHF exchange term $(\mu\lambda|\sigma\nu)^{LR}$ and of the XC potential matrix $\mathbf{V}^{\omega\omega'}_{XC}$. The former is defined by

$$(\mu\lambda|\sigma\nu)^{LR} = \int \chi^*_\mu(\mathbf{r}_1)\chi_\lambda(\mathbf{r}_1)\frac{\mathrm{erf}(\gamma\cdot r_{12})}{r_{12}}\chi^*_\sigma(\mathbf{r}_2)\chi_\nu(\mathbf{r}_2)d\mathbf{r}_1 d\mathbf{r}_2. \tag{46}$$

In CAM-B3LYP,[45] the two-electron Coulomb operator is divided into the short-range (SR) and LR parts using parameters a, b, and γ where γ determines the partitioning of space,

$$\frac{1}{r_{12}} = \frac{1 - [a + b\cdot \mathrm{erf}(\gamma\cdot r_{12})]}{r_{12}} + \frac{a + b\cdot \mathrm{erf}(\gamma\cdot r_{12})}{r_{12}}. \tag{47}$$

The XC potential matrices are given according to

$$V^{\alpha\alpha}_{\mu\nu,XC} = (\mu|\frac{\delta E_{XC}(\rho,m)}{\delta\rho} + \frac{\delta E_{XC}(\rho,m)}{\delta m}\frac{m_z}{m}|\nu), \tag{48}$$

$$V^{\beta\beta}_{\mu\nu,XC} = (\mu|\frac{\delta E_{XC}(\rho,m)}{\delta\rho} - \frac{\delta E_{XC}(\rho,m)}{\delta m}\frac{m_z}{m}|\nu), \tag{49}$$

$$V^{\beta\alpha}_{\mu\nu,XC} = (\mu|\frac{\delta E_{XC}(\rho,m)}{\delta m}\frac{(m_x + im_y)}{m}|\nu), \tag{50}$$

$$V^{\alpha\beta}_{\mu\nu,XC} = (\mu|\frac{\delta E_{XC}(\rho,m)}{\delta m}\frac{(m_x - im_y)}{m}|\nu). \tag{51}$$

Here, $E_{XC}(\rho,m)$ is the XC energy functional, ρ the electron density, $\mathbf{m}$ the magnetization density vector, and $m = |\mathbf{m}|$ the scalar magnetization density.[46] For the LC-DFT approach, the SR term is included in E_{XC}. In the cases of the pure-, hybrid-, and LC-DFT approaches, parameters $a = 0$, $b = 1$, $(\mu\lambda|\sigma\nu)^{LR} = 0$; $a \neq 0$, $b = 1$, $(\mu\lambda|\sigma\nu)^{LR} = 0$, and $a \neq 0$, $b \neq 0$, $(\mu\lambda|\sigma\nu)^{LR} \neq 0$ are used, respectively.

To obtain the first-order density matrix $\mathbf{P}^{(1)}_t$ at the GKS level, the first-order GKS matrix is defined as follows (compare with Eqs. (36)-(39)):

$$\begin{aligned} F^{(1)\alpha\alpha}_{\mu\nu,t} &= H^{(1)NESC,\alpha\alpha}_{\mu\nu,t} + \sum_{\sigma,\lambda}\left(P^{(1)\alpha\alpha}_{\sigma\lambda,t} + P^{(1)\beta\beta}_{\sigma\lambda,t}\right)(\mu\nu|\sigma\lambda) \\ &\quad - \sum_{\sigma,\lambda} P^{(1)\alpha\alpha *}_{\lambda\sigma,t}\left[a\,(\mu\lambda|\sigma\nu) + b(\mu\lambda|\sigma\nu)^{LR}\right] \\ &\quad + bV^{(1)\alpha\alpha}_{\mu\nu,XC,t}, \end{aligned} \tag{52}$$

$$\begin{aligned} F^{(1)\beta\beta}_{\mu\nu,t} &= H^{(1)NESC,\beta\beta}_{\mu\nu,t} + \sum_{\sigma,\lambda}\left(P^{(1)\alpha\alpha}_{\sigma\lambda,t} + P^{(1)\beta\beta}_{\sigma\lambda,t}\right)(\mu\nu|\sigma\lambda) \\ &\quad - \sum_{\sigma,\lambda} P^{(1)\beta\beta *}_{\lambda\sigma,t}\left[a\,(\mu\lambda|\sigma\nu) + b(\mu\lambda|\sigma\nu)^{LR}\right] \\ &\quad + bV^{(1)\beta\beta}_{\mu\nu,XC,t}, \end{aligned} \tag{53}$$

$$\begin{aligned} F^{(1)\beta\alpha}_{\mu\nu,t} &= H^{(1)NESC,\beta\alpha}_{\mu\nu,t} \\ &\quad - \sum_{\sigma,\lambda} P^{(1)\beta\alpha *}_{\lambda\sigma,t}\left[a\,(\mu\lambda|\sigma\nu) + b(\mu\lambda|\sigma\nu)^{LR}\right] \\ &\quad + bV^{(1)\beta\alpha}_{\mu\nu,XC,t}, \end{aligned} \tag{54}$$

$$\begin{aligned} F^{(1)\alpha\beta}_{\mu\nu,t} &= H^{(1)NESC,\alpha\beta}_{\mu\nu,t} \\ &\quad - \sum_{\sigma,\lambda} P^{(1)\alpha\beta *}_{\lambda\sigma,t}\left[a\,(\mu\lambda|\sigma\nu) + b(\mu\lambda|\sigma\nu)^{LR}\right] \\ &\quad + bV^{(1)\alpha\beta}_{\mu\nu,XC,t}. \end{aligned} \tag{55}$$

Here, $\mathbf{V}^{(1)\omega\omega'}_{XC,t}$ denotes the derivative of the XC potential matrix $\mathbf{V}^{\omega\omega'}_{XC}$ with respect to F_t. In this study we used the collinear approximation to obtain $\mathbf{V}^{(1)\omega\omega}_{XC,t}$, i.e.,

$$V^{(1)\omega\omega}_{\mu\nu,XC,t} = (\mu|\frac{\delta^2 E_{XC}(\rho)}{\delta\rho\delta\rho'}\frac{\partial\rho'}{\partial F_t}|\nu), \tag{56}$$

because the contribution of the non-collinear XC potentials is small for the calculation of valence properties.[47]

III. IMPLEMENTATION AND COMPUTATIONAL DETAILS

The equations and algorithm worked out above for calculating 2c-NESC electric dipole moment $\boldsymbol{\mu}$ and dipole polarizability $\boldsymbol{\alpha}$ were implemented into the NESC program of the *ab initio* package COLOGNE2016.[48]

As in previous work, the matrix $\mathbf{W}_{so}$ was scaled by suitable screening factors $\sqrt{Q(l_\mu)/Z_\mu}$ before the Dirac equation was solved and the 2c-NESC matrix was formed.[24] Scaling was exclusively performed with the mSNSO(W) method, which was shown in previous studies to provide an optimal choice in terms of accuracy and feasibility. We used $Q(d) = 11.0$, $Q(f) = 28.84$, $Q(l_\mu > 3) = l_\mu(l_\mu + 1)(2l_\mu + 1)/3$, and $Q(p) = 2.34\ Erf[(34\,500/\alpha_p)^2]$, where α_p is the Gaussian exponent of the p-type basis function.[24] In addition since $Q(l_\mu)$ may be overestimated for the basis functions with large l_μ, $Q(l_\mu)$ is then replaced by $Q'(l_\mu)$

$$Q'(l_\mu) = \begin{cases} Q(l_\mu) & (Z_\mu > Q(l_\mu)) \\ Q(l'_\mu) & (Z_\mu \le Q(l_\mu)) \end{cases}, \tag{57}$$

where l'_μ is the maximum l_μ value which makes $Z_\mu > Q(l'_\mu)$.

In contrast to the gradient calculations,[24] matrix $\mathbf{W}_{so}$ in $\partial\mathbf{W}/\partial F_t$ was not scaled by mSNSO since the two-electron SOC integrals do not contribute to an external electric field. The corrections of the mSNSO(W) method were only used for the 2c-calculations of the NESC wavefunction.

The accuracy of the analytically calculated 2c-NESC properties was tested by comparing results with those available at the 4c-HF and 4c-DFT level of theory using geometries and basis sets in a way that a direct comparison was meaningful. For this reason, all calculations of this work have been carried out with uncontracted basis sets listed in Table I. For comparison with 4c-DFT results, we used exchange-correlation functionals at the GDFT level of theory: (i) GGA functionals BLYP[49,50] and BP86,[49,51] (ii) hybrid functional PBE0[52,53] and the long-range corrected hybrid functional CAM-B3LYP.[45]

Benchmark calculations were carried out with a finite (F) nucleus presented by a Gaussian charge distribution.[1,54] For reasons of comparison, calculations with point (P) charge model of the nucleus were also carried out. In the following, symbols F and P will indicate which nuclear model has been employed. A value of 137.035 999 070(98) was used for the velocity of light c.[55]

The isotropic polarizability $\alpha(iso)$ and anisotropic polarizability $\alpha(aniso)$ were calculated using the following equations:

$$\alpha(iso) = 1/3(\alpha_{xx} + \alpha_{yy} + \alpha_{zz}), \tag{58}$$

$$\begin{aligned} \alpha(aniso) &= \sqrt{1/2}[(\alpha_{xx} - \alpha_{yy})^2 + (\alpha_{yy} - \alpha_{zz})^2 \\ &\quad + (\alpha_{zz} - \alpha_{xx})^2 + 6(\alpha^2_{xz} + \alpha^2_{xy} + \alpha^2_{yz})]^{1/2}, \end{aligned} \tag{59}$$

where the latter equation simplifies to Eq. (60) in case of molecules with high symmetry (as studied in this work):

$$\begin{aligned} \alpha(aniso) &= \sqrt{1/2}[(\alpha_{xx} - \alpha_{yy})^2 + (\alpha_{yy} - \alpha_{zz})^2 \\ &\quad + (\alpha_{zz} - \alpha_{xx})^2]^{1/2}. \end{aligned} \tag{60}$$

Differences between NR and scalar relativistic (spin-free: SF) properties are given by the quantity $\Delta SF = P(SF) - P(NR)$, where property P is either the electric dipole moment $\boldsymbol{\mu}$ or the electric dipole polarizability $\boldsymbol{\alpha}$. Similarly, the SOC correction for the property P is defined as $\Delta SO = P(SO) - P(SF)$. The Δ values will be influenced by the geometry and the basis set used. The best geometry available (experimental or calculated) was used at all levels of theory to largely exclude geometry effects on calculated dipole moments and polarizabilities. Noteworthy is that the

TABLE I. List of the uncontracted basis sets used in this study.

Basis B#	Element	Description	Reference
B1	H, F	aug-cc-pV5Z: H(9s 5p 4d 3f), F(15s 9p 5d)	66 and 67
	Cl	Sapporo-QZP-2012: (18s 12p 8d)	68
	Br, Ag, Au	Dyall's TZ: Br(23s 16p 10d 2f), Ag(28s 20p 13d 4f), Au(30s 24p 15d 11f)	69–72
	I	Dyall's DZ: (21s 16p 11d 3f)	72 and 73
B2	H, O, F, S, Cl, Se, Br, Te, I, Po, At	Sadlej pVTZ: H(6s 4p), O and F(10s 6p 4d), S and Cl(13s 10p 4d), Se and Br(15s 12p 9d), Te and I(19s 15p 12d 4f), Po and At (20s 17p 14d 5f)	74–78
B3	H	aug-cc-pV5Z: (9s 5p 4d 1f)	66
	Rg, Cn	Dyall's QZ: Rg(36s 35p 24d 16f 6g), Cn(36s 35p 24d 16f 3g)	72 and 79
B4	O, F, Cl, Ar	aug-cc-pVTZ: O and F(11s 6p 3d 2f), Cl and Ar(16s 10p 3d 2f)	66 and 80
	Kr, Xe, Au	Dyall's TZ: Kr(24s 17p 11d 2f), Xe(29s 22p 16d 2f), Au(30s 24p 15d 10f 1g)	69 and 71–73
B5	H, O, F, Cl	Sapporo-QZP-2012: H(9s 4p 3d 2f), O and F(13s 9p 5d 4f 3g), Cl(18s 12p 8d 5f 3g)	68, 81, and 82
	Br, Sn, I, Ge, Pb	Sapporo-DKH3-QZP-2012: Br(22s 16p 12d 6f 5g), Sn and I(25s 18p 14d 6f 5g), Ge(22s 16p 11d 6f 5g), Pb(29s 23p 17d 13f 5g)	68, 81, and 83
B6	Ti	aug-cc-pVTZ: (21s 15p 9d 3f 2g)	84
	Zr, Hf, Rf	Dyall's TZ: Zr(28s 20p 13d), Hf(30s 24p 15d 10f), Rf(32s 29p 20d 13f)	70–72 and 79
B7	Ca, Sr, Ba, Ag, Au	Sapporo-DKH3-QZP-2012: Ca(21s 15p 6d 4f 2g), Sr(23s 17p 13d 4f 2g), Ba(28s 21p 16d 3f 2g), Ag(23s 16p 13d 4f 3g), Au(27s 22p 17d 11f 3g)	68, 81, and 83
	Ra	Dyall's TZ: Ra(33s 29p 17d 11f)	72 and 85
B8	Mg, Ca	Sadlej pVTZ: Mg(13s 10p 4d), Ca(15s 13p 4d)	74–78
	Sr, Ba, Pb, Ra,	Dyall's TZ: Sr(29s 21p 12d 1f), Ba(31s 25p 15d 1f), Pb and Ra(34s 31p 18d 12f),	69 and 85
	Rn, Hg, Cn	Rn(31s 27p 18d 12f), Hg(30s 24p 15d 11f 2g), Cn(32s 29p 20d 13f 5g)	71, 72, and 79
	Yb, No	Dyall's QZ: Yb(35s 30p 19d 16f 3g), No(37s 34p 24d 15f 2g)	71, 72, and 79
B9	Cu	aug-cc-pVDZ-DK: (21s 17p 9d 3f)	84
	Ag, Au	Dyall's DZ: Ag(21s 14p 10d 3f), Au(24s 19p 12d 9f)	70–72
B10	H, O, F, Cl, Br	def2-QZVPP: H(7s 3p 2d 1f), O and F(15s 8p 3d 2f 1g), Cl(20s 14p 4d 2f 1g), Br(24s 20p 10d 4f 1g)	86
	I	Sapporo-DKH3-TZP-2012: (22s 18p 14d 3f)	68 and 81
	Ru	Sapporo-DKH3-QZP-2012: (23s 17p 13d 4f 3g)	68 and 81
	Os, Hg, U	SARC: Os(22s 15p 11d 6f), Hg(22s 15p 11d 6f 2g), U(29s 20p 16d 12f)	87 and 88
	Hs	Dyall's TZ: (32s 29p 20d 14f 2g)	72 and 79
B11	At	Sapporo-DKH3-QZP-2012: (29s 23p 17d 13f 5g)	81 and 83
	Cn	Dyall's QZ: (36s 35p 24d 15f)	72 and 79

NESC calculations in general, but especially in this work are carried out exclusively with uncontracted basis sets so that the different NR and relativistic contractions do not play any role and the analysis of relativistic effects on dipole moments and polarizabilities becomes meaningful.

IV. RESULTS AND DISCUSSION

The results of all benchmark calculations carried out at the 2c-NESC level and compared with the corresponding NR, 1c-, and 4c-values are summarized in Tables II–V. Additional data are given in the supplementary material. Table II compares the 2c-NESC/CAM-B3LYP and 2c-NESC/PBE0 dipole moments μ of polar diatomic molecules calculated with the corresponding NR, 1c-NESC, and experimental values. For this purpose, the changes ΔSF and ΔSO of μ are also listed. Atomic polarizabilities are compared in a similar way in Table III whereas molecular polarizabilities calculated in this work are given in Tables IV and V. In the latter cases, the polarizability tensor is characterized by isotropic (iso) and anisotropic (aniso) polarizability. To analyze the effects of SOC on dipole moments and polarizabilities, we will focus on the splitting of the frontier orbitals of a molecule and analyze their mixing under the impact of SOC (see Figures 1 and 2).

A. Discussion of 2c-NESC dipole moments

There are two opposing trends in the calculated relativistic corrections for the molecular dipole moments. For silver halogenides and gold halogenides, the scalar relativistic corrections decrease the value of the NR dipole moment and bring it in this way into better agreement with the experimental value. The SF correction is larger than the SO correction, which is ≤0.1 D (Table II). As the relativistic corrections increase with the atomic number (AN), they are larger for AuX than AgX. For the I-interhalogens and the tetrel oxides, the scalar relativistic corrections are all relatively small (≤0.4 D) and positive (Table II), i.e., the SF corrections increase the dipole moment. The SO correction can be both positive or negative. In the case of PbO, the SO correction (0.2 D) is comparable in magnitude to the scalar relativistic correction (−0.3 D; Table II).

TABLE II. Molecular electric dipole moments (D) calculated with 1c- and 2c-NESC methods.[a]

Method	Molecule	State	NR	1c-NESC	2c-NESC	Expt.	ΔSF	ΔSO	Basis	Nucleus model	R(AB) (Å)
CAM-B3LYP	AgF	$^1\Sigma^+$ (0)	6.19	5.84	5.84	6.22[58]	−0.35	0.00	B5,B7	F	1.983[89]
	AgCl	$^1\Sigma^+$ (0)	6.25	5.73	5.73	6.076[90]	−0.52	0.00	B5,B7	F	2.281[91]
	AgBr	$^1\Sigma^+$ (0)	6.10	5.47	5.45	5.620[92]	−0.63	−0.02	B5,B7	F	2.393[91]
	AgI	$^1\Sigma^+$ (0)	5.90	5.10	5.00	4.550[93]	−0.80	−0.10	B5,B7	F	2.545[91]
	AuF	$^1\Sigma^+$ (0)	5.51	4.29	4.22	4.13 ± 0.02[94]	−1.22	−0.07	B5,B7	F	1.918[95]
	AuCl	$^1\Sigma^+$ (0)	5.68	3.83	3.76	3.69 ± 0.02[96]	−1.85	−0.07	B5,B7	F	2.199[97]
	AuBr	$^1\Sigma^+$ (0)	5.60	3.45	3.41		−2.15	−0.04	B5,B7	F	2.318[97]
	AuI	$^1\Sigma^+$ (0)	5.48	2.96	2.87		−2.52	−0.09	B5,B7	F	2.471[98]
	IH	$^1\Sigma^+$ (0)	0.58	0.46	0.43	0.4476[99]	−0.12	−0.03	B5	F	1.609[100]
	IF	$^1\Sigma^+$ (0)	1.77	1.95	2.03	1.95[101]	0.18	0.08	B5	F	1.910[100]
	ICl	$^1\Sigma^+$ (0)	1.00	1.19	1.31	1.21[102]	0.19	0.12	B5	F	2.321[100]
	IBr	$^1\Sigma^+$ (0)	0.55	0.68	0.80	0.737[103]	0.12	0.12	B5	F	2.469[100]
	GeO	$^1\Sigma^+$ (0)	3.63	3.67	3.67	3.281[100]	0.04	0.00	B5	F	1.625[104]
	SnO	$^1\Sigma^+$ (0)	4.50	4.62	4.60	4.32[100]	0.12	−0.02	B5	F	1.833[104]
	PbO	$^1\Sigma^+$ (0)	4.79	5.12	4.89	4.65[100]	0.33	−0.23	B5	F	1.922[104]
PBE0	AgF	$^1\Sigma^+$ (0)	6.10	5.73	5.73	6.22[58]	−0.37	0.00	B5,B7	F	1.983[89]
	AgCl	$^1\Sigma^+$ (0)	6.17	5.62	5.62	6.076[90]	−0.55	0.00	B5,B7	F	2.281[91]
	AgBr	$^1\Sigma^+$ (0)	6.01	5.36	5.34	5.620[92]	−0.65	−0.02	B5,B7	F	2.393[91]
	AgI	$^1\Sigma^+$ (0)	5.79	4.99	4.89	4.550[93]	−0.80	−0.10	B5,B7	F	2.545[91]
	AuF	$^1\Sigma^+$ (0)	5.41	4.11	4.05	4.13 ± 0.02[94]	−1.30	−0.06	B5,B7	F	1.918[95]
	AuCl	$^1\Sigma^+$ (0)	5.59	3.68	3.62	3.69 ± 0.02[96]	−1.91	−0.06	B5,B7	F	2.199[97]
	AuBr	$^1\Sigma^+$ (0)	5.50	3.30	3.27		−2.20	−0.03	B5,B7	F	2.318[97]
	AuI	$^1\Sigma^+$ (0)	5.36	2.83	2.75		−2.53	−0.08	B5,B7	F	2.471[98]
	IH	$^1\Sigma^+$ (0)	0.58	0.47	0.44	0.4476[99]	−0.12	−0.03	B5	F	1.609[100]
	IF	$^1\Sigma^+$ (0)	1.63	1.81	1.88	1.95[101]	0.18	0.07	B5	F	1.910[100]
	ICl	$^1\Sigma^+$ (0)	0.92	1.10	1.21	1.21[102]	0.18	0.11	B5	F	2.321[100]
	IBr	$^1\Sigma^+$ (0)	0.49	0.61	0.72	0.737[103]	0.12	0.11	B5	F	2.469[100]
	GeO	$^1\Sigma^+$ (0)	3.44	3.49	3.49	3.281[100]	0.05	0.00	B5	F	1.625[104]
	SnO	$^1\Sigma^+$ (0)	4.27	4.38	4.37	4.32[100]	0.11	−0.01	B5	F	1.833[104]
	PbO	$^1\Sigma^+$ (0)	4.54	4.89	4.70	4.65[100]	0.35	−0.19	B5	F	1.922[104]

[a]F denotes finite nucleus calculations. ΔSF is the difference between 1c-NESC and NR, ΔSO the difference between 2c- and 1c-calculation. $R(AB)$ gives the bond length used. The Ω value is given in parentheses in the state column.

The first group of molecules is characterized by the relativistic contraction of the valence s- and p-orbitals of the metal, which participate in σ- and π-bonding orbitals (Figure 1). Generally, orbital contraction leads to an increase of the effective electronegativity of the metal, i.e., its coefficient increases, the charge transfer from metal to halogen X is reduced, and the dipole moment decreased. In the second group, antibonding σ or π orbitals (indicated by a star in Figure 1) are occupied. Because of the orthogonality of the orbitals and the larger electronegativity of X in all these cases, the ns or np coefficient of atom A (A = Sn, Pb, I) is larger than those of the corresponding X orbitals. Contraction of the bonding orbitals (the effective electronegativity and the orbital coefficient of A increase) implies that in the antibonding orbitals the coefficients of the A orbitals become smaller and the charge transfer is increased thus leading to a larger dipole moment. The SF effect associated with the antibonding orbitals is partly offset by the contraction of the bonding orbital and relatively small ΔSF values result (Table II).

Changes in the dipole moment are due to SO-splitting and spinor mixing. For the closed shell molecules considered, the changes caused by SO splittings cancel as $\pi_{1/2}$ and $\pi_{3/2}$ spinors are always pairwise (un)occupied. Relevant SOC effects result from a mixing of occupied and unoccupied spinors provided that they have the same ω-value, sufficient overlap, and are close in energy. Figure 1 shows a schematic presentation of the valence orbitals of molecule AX (A: atom with relatively large AN; X: halogen or oxygen) where scalar relativistic orbitals are assumed. The ordering of these orbitals will vary with the variation of AX. Schematically, the SO splittings of the valence orbitals and their occupation are shown on the right for different AX molecules where again orbital energies and ordering are only given schematically in Figure 1. The most likely interactions between occupied and unoccupied orbitals are indicated by a rectangular parenthesis. In all cases indicated, these interactions involve σ and π orbitals with $\omega = 1/2$. Three different situations can be observed.

At the left-hand side of the diagram in Figure 1, the scalar relativistic energies are shown and on the right-hand side the SO splittings are given for some examples. The latter diagrams are useful for discussing the SO-induced mixing of occupied and unoccupied spinors. In the case of the AgX and AuX molecules, the mixing takes place between an X dominated $\pi_{1/2}$ lone pair spinor and an A dominated $\sigma^{\star}_{1/2}$ spinor. Because of the latter, charge is relocated at A, the charge transfer from A to X is somewhat lower than in the scalar relativistic case, and accordingly, a slightly lower dipole moment results.

TABLE III. Calculated atomic polarizabilities (*bohr*^{3}) obtained with 1c- and 2c-NESC methods. The finite nucleus model and the B8 basis sets were used.

Method	Atom	State	NR	1c-NESC	2c-NESC	Reference 4c	Reference 4c-CCSD(T)	Expt.	ΔSF	ΔSO
HF	Mg	$^1S_0$	81.69	81.25	81.25	81.22[a]		59 ± 16[105]	−0.44	0.00
	Ca	$^1S_0$	185.17	182.54	182.54	182.45[a]		168.7[106]	−2.63	0.00
	Sr	$^1S_0$	245.78	232.53	232.51	232.54[a]		186.3[107]	−13.25	−0.02
	Ba	$^1S_0$	367.60	323.97	323.77	323.80[a]		267.9[107]	−43.63	−0.20
	Ra	$^1S_0$	440.62	299.42	297.12	296.77[a]			−141.20	−2.30
	Rn	$^1S_0$	33.95	32.63	34.73	34.99[a]			−1.32	2.10
	Hg	$^1S_0$	80.00	44.89	44.80	44.90[b]		33.919[61]	−35.11	−0.09
	Pb	$^3P_0$	58.32	46.80	49.65	49.91[b]		47.1 ± 7[108]	−11.52	2.85
	Cn	$^1S_0$	100.40	28.43	28.68	29.46[b]			−71.97	0.25
	Yb	$^1S_0$	230.03	179.17	178.67	179.49[c]		147.1 ± 19.6[105]	−50.86	−0.50
	No	$^1S_0$	286.24	145.24	141.73	142.65[c]			−141.00	−3.51
PBE0	Mg	$^1S_0$	75.38	74.97	74.97	74.99[d]		59 ± 16[105]	−0.41	0.00
	Ca	$^1S_0$	164.96	162.62	162.61	162.72[d]		168.7[106]	−2.34	−0.01
	Sr	$^1S_0$	213.94	202.85	202.83	202.71[d]		186.3[107]	−11.09	−0.02
	Ba	$^1S_0$	313.66	277.78	277.66	277.41[d]	272.8[e]	267.9[107]	−35.88	−0.12
	Ra	$^1S_0$	372.52	257.10	255.59	255.02[d]	242.8[e]		−115.42	−1.51
	Rn	$^1S_0$	34.74	34.07	36.25	36.63[d]			−0.67	2.18
	Hg	$^1S_0$	62.48	36.42	36.42		34.15[f]	33.919[61]	−26.06	0.00
	Pb	$^3P_0$	56.54	47.40	50.05		46.96[f]	47.1 ± 7[108]	−9.14	2.65
	Cn	$^1S_0$	78.91	26.21	26.52		27.64[f]		−52.70	0.31
	Yb	$^1S_0$	193.66	147.65	147.26		140.44[g]	147.1 ± 19.6[105]	−46.01	−0.39
	No	$^1S_0$	242.19	120.26	117.96		110.28[g]		−121.93	−2.30
CAM-B3LYP	Mg	$^1S_0$	71.87	71.47	71.47	71.46[h]		59 ± 16[105]	−0.40	0.00
	Ca	$^1S_0$	155.26	152.94	152.94	152.97[h]		168.7[106]	−2.32	0.00
	Sr	$^1S_0$	201.31	189.93	189.92	189.92[h]		186.3[107]	−11.38	−0.01
	Ba	$^1S_0$	296.56	259.64	259.56	259.50[h]	272.8[e]	267.9[107]	−36.92	−0.08
	Ra	$^1S_0$	352.10	236.82	236.05	235.71[h]	242.8[e]		−115.28	−0.77
	Rn	$^1S_0$	34.62	33.87	36.12	36.51[h]			−0.75	2.25
	Hg	$^1S_0$	60.91	36.45	36.47		34.15[f]	33.919[61]	−24.46	0.02
	Pb	$^3P_0$	54.77	45.71	47.45		46.96[f]	47.1 ± 7[108]	−9.06	1.74
	Cn	$^1S_0$	77.11	26.76	27.10		27.64[f]		−50.35	0.34
	Yb	$^1S_0$	180.90	136.04	135.73		140.44[g]	147.1 ± 19.6[105]	−44.86	−0.31
	No	$^1S_0$	226.00	109.29	107.77		110.28[g]		−116.71	−1.52

[a]4c-DHF values taken from Ref. 109.
[b]Reference 110.
[c]Reference 111.
[d]4c-PBE0 values from Ref. 109.
[e]4c-CCSD(T) values from Ref. 59.
[f]From Ref. 110.
[g]From Ref. 111.
[h]4c-CAM-B3LYP values from Ref. 109.

A different situation is given for SnO and PbO. The mixing of the occupied $\sigma^\star_{1/2}$ spinor with the unoccupied $\pi^\star_{1/2}$ spinor (Figure 1) leads to a stronger relocation of charge at A. Both spinors are characterized by a large A and a small O coefficient, but the ratio c_A/c_O is according to the Perturbational MO (PMO) theory[56] irreversibly proportional to the overlap of the atomic orbitals (spinors) and thereby smaller for the $\sigma^\star_{1/2}$ than the $\pi^\star_{1/2}$ spinor. Mixing of these spinors implies that charge is transferred back from O to A thus leading to the reduction of the molecular dipole moment and a better agreement with experiment (Table II).

For the interhalogen molecules, an occupied $\pi^\star_{1/2}$ spinor mixes with an unoccupied $\sigma^\star_{1/2}$ spinor (Figure 1) thus leading to the reverse situation as iodine is always the less electronegative element in the molecules investigated. The charge transfer is increased, which causes an increase rather than a decrease of the molecular dipole moment (Table II). According to PMO theory, the ratio c_A/c_O is obtained from dividing the overlap S by the orbital energy difference $\epsilon_I - \epsilon_X$. The latter decreases with decreasing electronegativity difference between I and X, which is related to the fact that the value ΔSO increases for the dipole moment from 0.08 to 0.12 D for X = F to X = Br (Table II).

2c-NESC dipole moments obtained with CAM-B3LYP are in somewhat better agreement with experiment than the corresponding PBE0 values (Table II), which is in line with observations made in other work.[57] However, in some cases the PBE0 results are slightly better. In general, agreement is satisfactory where the ΔSF and ΔSO corrections of the dipole moment are essential to get close to the experimental values for the molecules containing "relativistic" atoms with large AN. Noteworthy is that the measured value for AgF is clearly

TABLE IV. Static dipole polarizabilities ($bohr^3$) obtained with the 1c- and 2c-NESC methods.

Method	α	Molecule	State	NR	1c-NESC	2c-NESC	Reference	Expt.	ΔSF	ΔSO	Basis	Nucleus model	Bond length (Å)
BP86	iso	$TiCl_4$	$^1A_1$	100.48	100.27	100.29	100.3[a]	101.4[112]	−0.21	0.02	B6	F	2.187[113]
		$ZrCl_4$	$^1A_1$	104.65	103.59	103.63	103.6[a]		−1.06	0.04	B6	F	2.336[113]
		$HfCl_4$	$^1A_1$	101.98	99.10	99.18	99.3[a]		−2.88	0.08	B6	F	2.316[113]
		$RfCl_4$	$^1A_1$	107.10	100.90	101.13	101.2[a]		−6.20	0.23	B6	F	2.370[113]
		RuO_4	$^1A_1$	51.64	51.24	51.24	58.07[b]	58.6[61]	−0.40	0.00	B10	F	1.706[114]
		OsO_4	$^1A_1$	50.47	49.12	49.12	55.28[b]	55.1[61]	−1.35	0.00	B10	F	1.714[115]
		HsO_4	$^1A_1$	53.73	50.54	50.41	66.00[b]		−3.19	−0.13	B10	F	1.757[24]
		UF_6	$^1A_{1g}$	61.28	54.95	54.84		53.5[62]	−6.33	−0.11	B10	F	1.990[24]
PBE0	iso	$TiCl_4$	$^1A_1$	95.55	95.30	95.32	100.3[a]	101.4[112]	−0.25	0.02	B6	F	2.187[113]
		$ZrCl_4$	$^1A_1$	99.13	98.05	98.07	103.6[a]		−1.08	0.02	B6	F	2.336[113]
		$HfCl_4$	$^1A_1$	96.61	93.73	93.79	99.3[a]		−2.88	0.06	B6	F	2.316[113]
		$RfCl_4$	$^1A_1$	101.56	95.41	95.65	101.2[a]		−6.15	0.24	B6	F	2.370[113]
		RuO_4	$^1A_1$	50.85	50.42	50.42		58.6[61]	−0.44	0.00	B10	F	1.706[114]
		OsO_4	$^1A_1$	49.53	48.09	48.10		55.1[61]	−1.44	0.01	B10	F	1.714[115]
		HsO_4	$^1A_1$	52.38	49.02	48.86			−3.36	−0.16	B10	F	1.757[24]
		UF_6	$^1A_{1g}$	58.10	51.08	50.99		53.5[62]	−7.02	−0.09	B10	F	1.990[24]

[a]X2C-BP86 value taken from Ref. 113.
[b]4c-BP86 values taken from Ref. 116.

too large (6.22 D[58]) whereas all calculated values suggest a dipole moment of 5.8 D (Table II).

B. Discussion of 2c-NESC atomic polarizabilities

The polarizability is a volume property reflected by the fact that its dimension is [length unit]^3. A large expansion of the atomic electron density into space implies a relatively large covalent radius and polarizability $\boldsymbol{\alpha}$. Hence, any change in the spatial extent of the electron density distribution caused by scalar relativistic effects leads to a change in the polarizability of atom A. SOC causes a splitting of the orbitals $l \geq 1$ where the p-orbitals with $j = 1/2$ are contracted and those with $j = 3/2$ are expanded. Hence, the SO splittings can be used to explain the ΔSO values of the atomic polarizabilities obtained in this work (Table III). Relatively large ΔSO values are obtained for Pb (6.11 bohr^3), Rn (−2.18), Ra (1.51), and No (2.30; Table III) where for Pb and Rn the SO correction is comparable or even larger than the SF correction. Noteworthy is that at the HF level the 2c-NESC value of α agrees well with the 4c-Dirac value (Table III). In the following, some groups of atoms are discussed in detail.

The NESC α-values of the earth alkali atoms increase from Mg (AN: 12; $\alpha = 81.7$ bohr^3) to Ra (AN: 88; 440.6 bohr^3, Table III). With increasing α the scalar relativistic correction becomes larger (from $|-0.44|$ to $|-141.2|$ bohr^3) as does the SO correction (from 0 to $|-2.3|$ bohr^3). The former is a direct consequence of the contraction of the ns electron density, which reduces the polarizability. Since SOC is in general small when there is no fractional occupation of p, d, or f orbitals, SOC leads to only minor corrections for Ba and Ra (−0.2 and −2.3 bohr^3), which are less than 1% of the total value (Table III). However, these corrections are essential for bringing the 1c-NESC/HF results in agreement with the 4c-DHF (Dirac HF) values. The ΔSO values reflect a (small) contraction of the valence s-orbital caused by SOC (Table III).

The SO corrections are the result of the SO splitting of the fully occupied (n-1)p- and (n-2)d-orbitals. Since the (n-1)$p_{3/2}$ and (n-2)$d_{5/2}$ spinors expand and are more diffuse, screening of the nuclear charge is slightly reduced. The effective nuclear charge for the ns electrons becomes somewhat larger. This leads to a small, but for Ra significant, contraction of the ns-electron density and a subsequent decrease of the atomic polarizability (Table III). Similar explanations hold for Hg and Cn (Eka-Hg) as well as Yb and No atoms that have ns^2 or ns^2 (n-2)f^{14} valence electron configurations. The scalar relativistic correction is too large (or the positive SOC correction too small) to exactly reproduce the 4c-DHF values. However, deviations are less than 1%, which is in line with the accuracy achieved with the mSNSO method.[23]

Noteworthy are the relativistic corrections obtained for Rn ($^1S_0$) and Pb ($^3P_0$) where for the noble gas the SO correction (2.10 bohr^3) is larger than the scalar relativistic correction (−1.32 bohr^3). This suggests that orbital contraction in the $6s^26p^6$ noble gas configuration is moderate and the SO splitting into $6p_{1/2}$ and into $6p_{3/2}$ spinors leads to an overall expansion of the electron density thus causing an increase in the polarizability $\boldsymbol{\alpha}$. This is in line with the negative ΔSO values for group 2 and group 12 elements (Table III).

For the Pb atom in its $^3P_0$ ground state, the calculated ΔSF and ΔSO values are −11.52 and 2.85 bohr^3. Both the 6s(Pb)- and 6p(Pb)-orbitals are contracted where the latter contraction is SO-averaged. Of the corresponding spinors $6s_{1/2}$, $6p_{1/2}$, and $6p_{3/2}$, only the first two are contracted whereas the third expands. Accordingly, the scalar relativistic $\alpha(iso)$-value is reduced, but much less than for example the corresponding Hg value because for the 6p orbital contraction is moderate. The increase of $\alpha(iso)$ caused by SOC is due to the $6p_{3/2}$ spinor and its expansion.

4c-DHF and 2c-NESC/HF values do not include electron correlation effects and therefore exaggerate atomic polarizabilities (Table III). The two hybrid functionals PBE0 and CAM-B3LYP, which include electron correlation, provide

TABLE V. Isotropic (iso) polarizabilities and polarizability anisotropies (aniso) in *bohr*^{3} calculated with 1c- and 2c-NESC methods.[a]

Method	α	Molecule	State	NR	1c-NESC	2c-NESC	Expt.	ΔSF	ΔSO	Basis	$R(AB)$ (Å)
PBE0	iso	HgH_2	$^1\Sigma_g^+$ (0)	37.22	34.53	34.40		−2.69	−0.13	B10	1.635[24]
		HgF_2	$^1\Sigma_g^+$ (0)	26.12	27.82	27.91		1.70	0.09	B10	1.909[24]
		$HgCl_2$	$^1\Sigma_g^+$ (0)	55.26	57.77	57.78		2.51	0.01	B10	2.247[24]
		$HgBr_2$	$^1\Sigma_g^+$ (0)	70.42	73.95	73.93		3.53	−0.02	B10	2.383[24]
		HgI_2	$^1\Sigma_g^+$(0)	107.49	112.5	113.0		5.01	0.48	B10	2.573[24]
		HgH_4	$^1A_{1g}$	45.83	43.71	43.58		−2.12	−0.13	B10	1.623[24]
		HgF_4	$^1A_{1g}$	42.53	40.66	40.54		−1.87	−0.12	B10	1.882[24]
		$HgCl_4$	$^1A_{1g}$	110.35	106.65	106.34		−3.70	−0.31	B10	2.293[24]
		IH	$^1\Sigma^+$ (0)	36.19	36.14	36.29	34.25 ~ 35.30[117]	−0.05	0.15	B5,B11	1.609[100]
		IF	$^1\Sigma^+$ (0)	34.99	34.79	34.78		−0.20	−0.01	B5,B11	1.910[100]
		ICl	$^1\Sigma^+$ (0)	49.42	49.38	49.55		−0.04	0.17	B5,B11	2.321[100]
		IBr	$^1\Sigma^+$ (0)	57.23	57.29	57.72		0.06	0.43	B5,B11	2.469[100]
		I_2	$^1\Sigma_g^+$ (0)	70.66	70.71	71.79	69.7 ± 1.8[118]	0.05	1.08	B5,B11	2.666[100]
		At_2	$^1\Sigma_g^+$ (0)	92.06	91.81	101.57		−0.25	9.76	B5,B11	3.046[119]
		Cn_2	$^1\Sigma_g^+$ (0)	187.58	58.78	61.73		−128.80	2.95	B5,B11	3.255[24]
	aniso	HgH_2	$^1\Sigma_g^+$ (0)	7.69	16.44	16.00		8.75	−0.44	B10	1.635[24]
		HgF_2	$^1\Sigma_g^+$ (0)	11.41	16.38	16.31		4.97	−0.07	B10	1.909[24]
		$HgCl_2$	$^1\Sigma_g^+$ (0)	39.10	51.06	51.02		11.96	−0.04	B10	2.247[24]
		$HgBr_2$	$^1\Sigma_g^+$ (0)	56.18	72.58	72.43		16.40	−0.15	B10	2.383[24]
		HgI_2	$^1\Sigma_g^+$ (0)	76.80	101.36	102.17		24.56	0.81	B10	2.573[24]
		HgH_4	$^1A_{1g}$	20.81	21.88	21.65		1.07	−0.23	B10	1.623[24]
		HgF_4	$^1A_{1g}$	30.12	26.69	26.42		−3.43	−0.27	B10	1.882[24]
		$HgCl_4$	$^1A_{1g}$	79.63	75.06	74.58		−4.57	−0.48	B10	2.293[24]
		IH	$^1\Sigma_g^+$ (0)	2.19	1.96	2.08		−0.23	0.12	B5,B11	1.609[100]
		IF	$^1\Sigma_g^+$ (0)	4.61	4.32	4.48		−0.29	0.16	B5,B11	1.910[100]
		ICl	$^1\Sigma_g^+$ (0)	24.06	23.75	24.28		−0.31	0.53	B5,B11	2.321[100]
		IBr	$^1\Sigma_g^+$ (0)	31.61	31.16	32.30		−0.45	1.14	B5,B11	2.469[100]
		I_2	$^1\Sigma_g^+$ (0)	41.96	41.19	43.89	45.1 ± 2.3[118]	−0.77	2.70	B5,B11	2.666[100]
		At_2	$^1\Sigma_g^+$ (0)	62.69	59.27	79.84		−3.42	20.57	B5,B11	3.046[119]
		Cn_2	$^1\Sigma_g^+$ (0)	164.11	28.29	35.13		−135.82	6.84	B5,B11	3.255[24]
CAM-B3LYP	iso	HgH_2	$^1\Sigma_g^+$ (0)	36.76	34.41	34.29		−2.35	−0.12	B10	1.635[24]
		HgF_2	$^1\Sigma_g^+$ (0)	25.78	27.56	27.65		1.78	0. 09	B10	1.909[24]
		$HgCl_2$	$^1\Sigma_g^+$ (0)	54.75	57.43	57.44		2.68	0.01	B10	2.247[24]
		$HgBr_2$	$^1\Sigma_g^+$ (0)	69.58	73.40	73.38		3.82	−0.02	B10	2.383[24]
		HgI_2	$^1\Sigma_g^+$ (0)	106.28	111.75	112.34		5.47	0.59	B10	2.573[24]
		HgH_4	$^1A_{1g}$	45.95	43.78	43.65		−2.17	−0.13	B10	1.623[24]
		HgF_4	$^1A_{1g}$	43.03	40.93	40.78		−2.10	−0.15	B10	1.882[24]
		$HgCl_4$	$^1A_{1g}$	113.25	108.63	108.25		−4.62	−0.38	B10	2.293[24]
		IH	$^1\Sigma_g^+$ (0)	36.06	35.97	36.14	34.25 ~ 35.30[117]	−0.09	0.17	B5,B11	1.609[100]
		IF	$^1\Sigma_g^+$ (0)	34.76	34.51	34.50		−0.25	−0.01	B5,B11	1.910[100]
		ICl	$^1\Sigma_g^+$ (0)	49.39	49.34	49.54		−0.05	0.20	B5,B11	2.321[100]
		IBr	$^1\Sigma_g^+$ (0)	57.21	57.29	57.78		0.08	0.49	B5,B11	2.469[100]
		I_2	$^1\Sigma_g^+$ (0)	70.54	70.63	71.87	69.7 ± 1.8[118]	0.09	1.24	B5,B11	2.666[100]
		At_2	$^1\Sigma_g^+$ (0)	92.15	92.04	103.35		−0.11	11.31	B5,B11	3.046[119]
		Cn_2	$^1\Sigma_g^+$ (0)	184.53	59.29	61.99		−125.24	2.70	B5,B11	3.255[24]
	aniso	HgH_2	$^1\Sigma_g^+$ (0)	7.79	16.12	15.69		8.33	−0.43	B10	1.635[24]
		HgF_2	$^1\Sigma_g^+$ (0)	11.00	15.86	15.79		4.86	−0.07	B10	1.909[24]
		$HgCl_2$	$^1\Sigma_g^+$ (0)	38.55	50.51	50.47		11.96	−0.04	B10	2.247[24]
		$HgBr_2$	$^1\Sigma_g^+$ (0)	55.46	72.12	72.00		16.66	−0.12	B10	2.383[24]
		HgI_2	$^1\Sigma_g^+$ (0)	74.84	100.30	101.34		25.46	1.04	B10	2.573[24]
		HgH_4	$^1A_{1g}$	21.24	21.98	21.75		0.74	−0.23	B10	1.623[24]
		HgF_4	$^1A_{1g}$	30.80	27.06	26.76		−3.74	−0.30	B10	1.882[24]
		$HgCl_4$	$^1A_{1g}$	84.34	78.30	77.71		−6.04	−0.59	B10	2.293[24]
		IH	$^1\Sigma_g^+$ (0)	2.39	2.20	2.34		−0.19	0.14	B5,B11	1.609[100]
		IF	$^1\Sigma_g^+$ (0)	4.82	4.55	4.73		−0.27	0.18	B5,B11	1.910[100]
		ICl	$^1\Sigma_g^+$ (0)	24.43	24.23	24.83		−0.20	0.60	B5,B11	2.321[100]
		IBr	$^1\Sigma_g^+$ (0)	32.17	31.90	33.21		−0.27	1.31	B5,B11	2.469[100]
		I_2	$^1\Sigma_g^+$ (0)	42.63	42.23	45.37	45.1 ± 2.3[118]	−0.40	3.14	B5,B11	2.666[100]

TABLE V. (*Continued.*)

Method	α	Molecule	State	NR	1c-NESC	2c-NESC	Expt.	ΔSF	ΔSO	Basis	$R(AB)$ (Å)
		At_2	$^1\Sigma_g^+$ (0)	65.23	62.96	87.52		−2.27	24.56	B5,B11	3.046[119]
		Cn_2	$^1\Sigma_g^+$ (0)	161.97	27.95	33.93		−134.02	5.98	B5,B11	3.255[24]

[a]F denotes finite nucleus calculations. ΔSF is the difference between 1c-NESC and NR, ΔSO the difference between 2c- and 1c-NESC calculation. $R(AB)$ gives the bond length used. The value of Ω is given in parentheses in the state column.

polarizabilities at the 2c-NESC level that are closer to experimental values or those of high level calculations such as 4c-CCSD(T).[59] For the atomic polarizabilities of Ra, Hg, Pd, Cn, Yb, and No, the 2c-NESC/CAM-B3LYP values are closer to the 4c-CCSD(T) values[59] than the 2c-NESC/PBE0 values. However, the latter are in better agreement with experiment.

C. Discussion of 2c-NESC molecular polarizabilities

In the case of polyatomic molecules, it is useful to discuss the isotropic polarizability $\alpha(iso)$ and the anisotropic polarizability $\alpha(aniso)$ given in Eqs. (58) and (60). In Table IV, $\alpha(iso)$ values of molecules ACl_4 (A = Ti, Zr, Hf, Rf), AO_4 (A = Ru, Os, Hs) and UF_6 calculated at the NR, 1c-NESC, and 2c-NESC levels of theory with XC functionals BP86 and PBE0 are shown. Again, the scalar relativistic correction of the occupied ns and np orbitals dominates thus leading to negative ΔSF values although they are moderate compared to some of the ΔSF changes of the atoms (Table IV). Changes in $\alpha(iso)$ upon scalar relativistic or SOC corrections are similar for the two XC functionals and therefore only the PBE0 results are discussed here.

Ti, Zr, Hf, and Rf have an ns^2 (n-1)d^2 electron configuration (Rf: $7s^2 5f^{14} 6d^2$), i.e., the LUMO and other low-lying virtual orbitals (e- and t_2-symmetrical) have relatively large (n-1) $d_{3/2}$- and $d_{5/2}$ contributions, which are more expanded into space than the (n-1) $p_{1/2}$ and $p_{3/2}$ spinors. The d(A)-orbitals make a significant contribution to the a_1-symmetrical LUMO and the following LUMO+1 orbitals of t_2-symmetry. Accordingly, the isotropic polarizability of these molecules slightly increases when SOC is included (for $RfCl_4$ by 0.24 $bohr^3$).

For AO_4 (A = Ru, Os, Hs), the electronegativity difference between A and O is larger than that between A and Cl in the case of the ACl_4 (A = Ti, Zr, Hf, Rf) molecules. Therefore, the SOC leads to a mixing of an orbital with almost no A contribution with one with little $2p\pi$ (O) or lp(O) contribution (lp: lone pair; Figure 2), which causes a small contraction and a reduction of the isotropic polarizability. Since the effects are small (driven by small changes in the electronegativities: e.g., $\chi(Hf) = 1.23$; $\chi(Cl) = 2.83$; difference $\Delta\chi = 1.60$; $\chi(Os) = 1.52$; $\chi(O) = 3.50$; $\Delta\chi = 1.98$[60]), the changes in $\alpha(iso)$ are also small (HsO_4, ΔSO: −0.16 $bohr^3$, Table IV). The same holds for UF_6 (U: $(Rn)7s^2 5f^3 6d^1$) where SOC leads to a mixing between

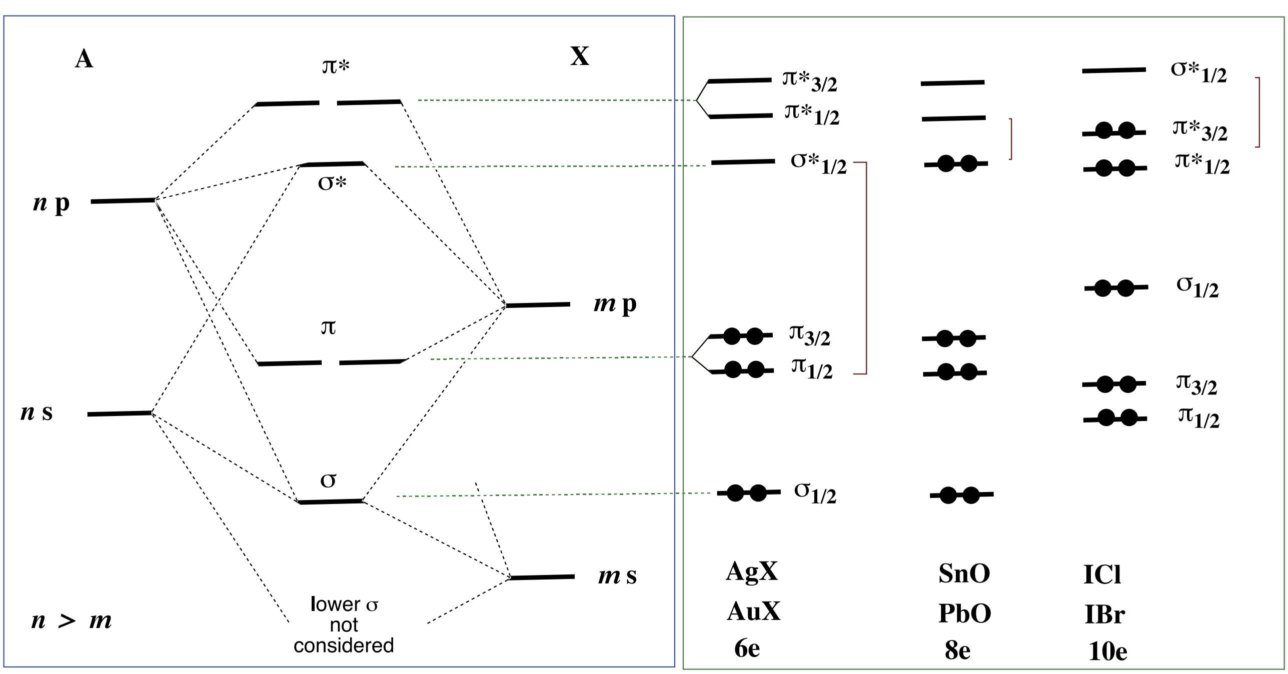

FIG. 1. Schematic representation of the orbital diagram of some diatomic molecules investigated and the SO coupling-induced splitting into spinors. The ω-value is indicated. (n and m give the principal quantum numbers of the frontier orbitals shown: ke: number of electrons; a star denotes an antibonding spinor. The frontier spinors that can mix under the impact of SOC are connected by a rectangular bracket.)

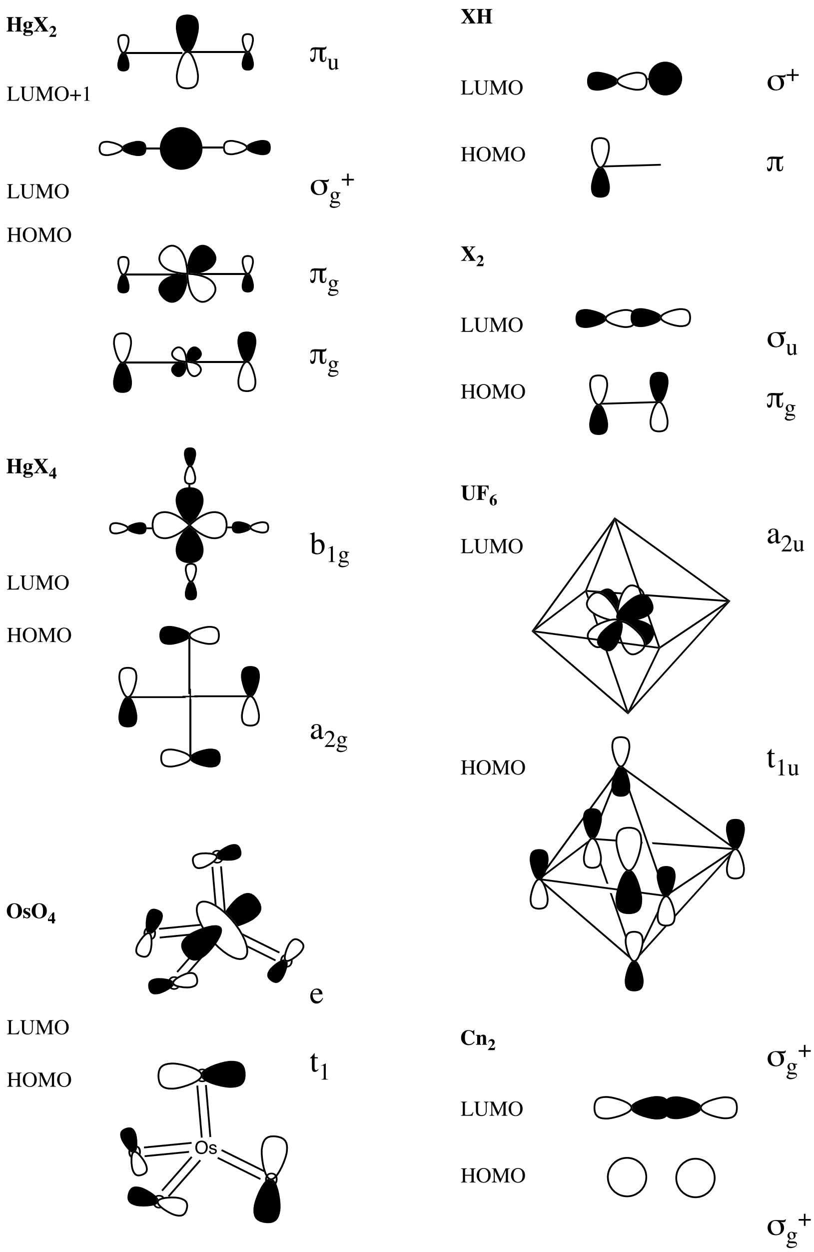

FIG. 2. Schematic representation of the frontier orbitals of some of the molecules investigated.

the t_{1u}-symmetrical HOMOs and the a_{2u}-symmetrical LUMO (Figure 2). The former is dominated by the lp(F) orbitals and the latter by a 5f(U)-orbital with only little lp(F) contributions (Figure 2). This causes the total electron density distribution to slightly contract thus leading to a ΔSO of -0.09 bohr^3 for the isotropic polarizability of UF_6.

In Table V, the $\alpha(iso)$ and $\alpha(aniso)$ values of mercury molecules HgX_n (X = H, F, Cl, Br, I; n = 2 or 4), (inter)halogens XX (XY) (X = I, At; Y = H, F, Cl, Br, I, At), and Cn_2 obtained with different methods are compared. Although scalar relativistic corrections are in general small, it is interesting that ΔSF is positive for the mercury dihalides. Since ΔSF is negative for HgH_2 as it should be in view of the contraction of the 6s(Hg)-orbital, the reason for the positive values must be a result of the lp(X)-orbitals that can mix with the 5d(Hg) orbitals (the 6p(Hg) orbitals are too high in energy) in a bonding and antibonding fashion (each being degenerate) where the latter correspond to the π_g HOMOs (Figure 2). For the antibonding π_g, the coefficient of the 5d(Hg) orbital is large and becomes larger because of scalar relativistic effects. Hence, the electron density expands in the x,y-directions, which causes a larger value of $\alpha(iso)$. The effect is larger the better the overlap between the 5d(Hg) and the lp(X) orbitals is, which increases from 2p(F) to 5p(I). The strong increase in the $\alpha(aniso)$ values reveals that the different density changes in π and σ direction lead to an overall stronger density anisotropy and a larger $\alpha(aniso)$ value.

For the HgX_4 molecules, the HOMO is of a_{2g} symmetry and also formed by the lp(X) orbitals (Figure 2). Because of symmetry, there cannot be any 5d(Hg) contribution. Therefore, the contraction of the 6s(Hg) orbital and the corresponding a_{1g}-symmetrical σ-orbital is dominant and leads to a negative ΔSF. This is confirmed by the corresponding HgH_4 value, which is also negative and of similar magnitude, thus confirming that the 6s(Hg) contraction is dominant.

For UF_6, there are two significantly different experimental polarizabilities, 84.4[61] and 53.5 bohr^3,[62] have been reported. This work indicates that the former value is outdated[63] and has to be replaced by the latter one, which is supported by 2c-NESC values of Table IV.

For the XX and XY molecules (X = I, At; Y = H, F, Cl, Br, I, At) scalar relativistic effects changing $\alpha(iso)$ are small. In these cases, ΔSO becomes significantly large for I_2 and At_2 (1.08 and 9.76 bohr^3, Table V). This is due to a splitting of the π_g HOMOs into $\pi_{g\,1/2}$ and $\pi_{g\,3/2}$ where the latter spinors expand and lead to a larger $\alpha(iso)$ value. HOMO and LUMO cannot interact because of the different inversional symmetries (Figure 2). The ΔSO values of the HgX_2 and HgX_4 molecules investigated are relatively small. They can be explained using the orbital pictures shown in Figure 2. The experimental polarizability of $HgCl_2$[61] is significantly larger than the calculated ones. As in the case of UF_6, this experimental value might be outdated.[63]

For the van der Waals complex Cn_2, a strong scalar relativistic decrease of $\alpha(iso)$ by -128.8 bohr^3 is calculated, which is due to the strong contraction of the $7s\sigma$ orbital (Figure 2). The SF-correction overshoots, which must be compensated by the SO correction. The latter leads to a mixing of the σ_g^+-symmetrical HOMO and the σ_g^+-symmetrical LUMO, which is much more expanded because of the $7p\sigma$ contributions to the latter orbital (Figure 2). Hence, $\alpha(iso)$ increases by 2.9 bohr^3 (Table V) where this increase is relatively small when compared with the increase calculated for At_2 (24.56 bohr^3, Table V). The moderate enlargement of $\alpha(iso)$ for Cn_2 is due to the fact that the HOMO contains a large contribution of $6d_{5/2}$ and has only a minor $7s_{1/2}$ contribution (contrary to what is shown in Figure 2) which in turn results from SO splitting and a change in the spinor ordering ($7s_{1/2}$ below $6d_{1/2}$).[64]

The 2c-NESC/PBE0 method produces the experimental values somewhat better than the 2c-NESC/CAM-B3LYP method for most of the molecules, although it is known that NR/CAM-B3LYP provides values comparable to those of NR/CCSD(T).[65] Generally, the scalar relativistic effect is more important than the SO effect in a polarizability calculation, but for the At_2 polarizability the SO effect turns out to be clearly dominant. The SO effect for At_2 is 9.6% of the 2c-NESC value.

V. CONCLUSIONS

The analytical gradient and Hessian of the 2c-NESC/mSNSO method with regard to the electric field components were developed, programmed, and implemented in a general purpose *ab initio* program. As first order response properties molecular dipole moments and as second order response properties atomic and molecular static dipole polarizabilities were calculated and analyzed. In those cases where a comparison with 4c calculations was possible, an almost exact reproduction of dipole moment, isotropic polarizability, and polarizability anisotropy values was achieved at the 2c-NESC/mSNSO level. SOC corrections for the electrical properties considered are in general small, for closed shell molecules but become relevant for molecules containing sixth and/or seventh period elements. Magnitude and trends in the SOC correction are successfully explained considering the mixing of frontier orbitals. Noteworthy is that the SO effect of At_2 is almost 10% of the 2c-NESC isotropic polarizability.

SUPPLEMENTARY MATERIAL

See the supplementary material for one table with calculated dipole moments and two tables with calculated polarizabilities.

ACKNOWLEDGMENTS

We acknowledge fruitful discussions with Professor Michael Filatov, SMU, Dallas. This work was financially supported by the National Science Foundation, Grant Nos. CHE 1464906 and CHE 1152357. We thank SMU for providing computational resources.

[1]K. G. Dyall and K. Fægri, *Introduction to Relativistic Quantum Chemistry* (Oxford University Press, Oxford, 2007).
[2]C. M. Marian, Wiley Interdiscip. Rev.: Comput. Mol. Sci. **2**, 187 (2012).
[3]P. A. M. Dirac, Proc. R. Soc. A **117**, 610 (1928).
[4]P. A. M. Dirac, Proc. R. Soc. A **123**, 714 (1929).
[5]K. G. Dyall, J. Chem. Phys. **106**, 9618 (1997).
[6]W. Zou, M. Filatov, and D. Cremer, Theor. Chem. Acc. **130**, 633 (2011).
[7]W. Zou, M. Filatov, and D. Cremer, J. Chem. Phys. **134**, 244117 (2011).
[8]W. Zou, M. Filatov, and D. Cremer, J. Chem. Phys. **137**, 084108 (2012).
[9]M. Filatov, W. Zou, and D. Cremer, J. Phys. Chem. A **116**, 3481 (2012).
[10]M. Filatov, W. Zou, and D. Cremer, J. Chem. Theory Comput. **8**, 875 (2012).
[11]M. Filatov, W. Zou, and D. Cremer, J. Chem. Phys. **137**, 054113 (2012).
[12]W. Zou, M. Filatov, and D. Cremer, J. Chem. Theory Comput. **8**, 2617 (2012).
[13]W. Zou, M. Filatov, D. Atwood, and D. Cremer, Inorg. Chem. **52**, 2497 (2013).
[14]M. Filatov, W. Zou, and D. Cremer, J. Chem. Phys. **137**, 131102 (2012).
[15]E. Kraka, W. Zou, M. Freindorf, and D. Cremer, J. Chem. Theory Comput. **8**, 4931 (2012).
[16]T. R. Furlani and H. F. King, J. Chem. Phys. **82**, 5577 (1985).
[17]D. G. Fedorov, S. Koseki, M. W. Schmidt, and M. S. Gordon, Int. Rev. Phys. Chem. **22**, 551 (2003).
[18]W. Liu, Mol. Phys. **108**, 1679 (2010).
[19]T. Saue, ChemPhysChem **12**, 3077 (2011).
[20]D. Peng and M. Reiher, Theor. Chem. Acc. **131**, 1081 (2012).
[21]T. Fleig, Chem. Phys. **395**, 2 (2012).
[22]M. Reiher and A. Wolf, *Relativistic Quantum Chemistry, The Fundamental Theory of Molecular Science*, 2nd ed. (Wiley-VCH, Weinheim, 2015).
[23]M. Filatov, W. Zou, and D. Cremer, J. Chem. Phys. **139**, 014106 (2013).
[24]W. Zou, M. Filatov, and D. Cremer, J. Chem. Phys. **142**, 214106 (2015).
[25]H. Fukui and T. Baba, J. Chem. Phys. **117**, 7836 (2002).
[26]S. K. Wolff and T. Ziegler, J. Chem. Phys. **109**, 895 (1998).
[27]J. Autschbach and T. Ziegler, J. Chem. Phys. **113**, 9410 (2000).
[28]J. Autschbach, J. Chem. Phys. **129**, 094105 (2008).
[29]Q. Sun, Y. Xiao, and W. Liu, J. Chem. Phys. **137**, 174105 (2012).
[30]F. Wang and W. Liu, J. Chin. Biochem. Soc. **50**, 597 (2003).
[31]J. Gao, W. Zou, W. Liu, Y. Xiao, D. Peng, B. Song, and C. Liu, J. Chem. Phys. **123**, 054102 (2005).
[32]D. Peng, W. Zou, and W. Liu, J. Chem. Phys. **123**, 144101 (2005).
[33]H. Iikura, T. Tsuneda, T. Yanai, and K. Hirao, J. Chem. Phys. **115**, 3540 (2001).
[34]T. Tsuneda and K. Hirao, Wiley Interdiscip. Rev.: Comput. Mol. Sci. **4**, 375 (2014).
[35]M. Filatov, W. Zou, and D. Cremer, Int. J. Quantum Chem. **114**, 993 (2014).
[36]D. Cremer, W. Zou, and M. Filatov, Wiley Interdiscip. Rev.: Comput. Mol. Sci. **4**, 436 (2014).
[37]W. Liu and D. Peng, J. Chem. Phys. **131**, 031104 (2009).
[38]W. Kutzelnigg and W. Liu, J. Chem. Phys. **123**, 241102 (2005).
[39]W. Liu and W. Kutzelnigg, J. Chem. Phys. **126**, 114107 (2007).

[40]W. Liu and D. Peng, J. Chem. Phys. **125**, 149901 (2006).
[41]W. Liu, Phys. Rep. **537**, 59 (2014).
[42]M. Filatov and D. Cremer, J. Chem. Phys. **119**, 1412 (2003).
[43]P. Pulay, Chem. Phys. Lett. **73**, 393 (1980).
[44]P. Pulay, J. Comput. Chem. **3**, 556 (1982).
[45]T. Yanai, D. P. Tew, and N. C. Handy, Chem. Phys. Lett. **393**, 51 (2004).
[46]F. Wang and T. Ziegler, Int. J. Quantum Chem. **106**, 2545 (2006).
[47]C. van Wüllen, J. Comput. Chem. **22**, 779 (2002).
[48]E. Kraka, W. Zou, M. Filatov, T. Yoshizawa, J. Gräfenstein, D. Izotov, J. Gauss, Y. He, A. Wu, V. Polo, L. Olsson, Z. Konkoli, Z. He, and D. Cremer, COLOGNE16, 2016.
[49]A. D. Becke, Phys. Rev. A **38**, 3098 (1988).
[50]C. Lee, W. Yang, and R. G. Parr, Phys. Rev. B **37**, 785 (1988).
[51]J. P. Perdew, Phys. Rev. B **33**, 8822 (1986).
[52]J. P. Perdew, K. Burke, and M. Ernzerhof, Phys. Rev. Lett. **77**, 3865 (1996).
[53]C. Adamo and V. Barone, J. Chem. Phys. **110**, 6158 (1999).
[54]L. Visscher and K. G. Dyall, At. Data Nucl. Data Tables **67**, 207 (1997).
[55]G. Gabrielse, D. Hanneke, T. Kinoshita, M. Nio, and B. Odom, Phys. Rev. Lett. **97**, 030802 (2006).
[56]B. M. Gimarc, *Molecular Structure and Bonding, The Qualitative Molecular Orbital Approach* (Academic Press, New York, 1979).
[57]E. Goll and H. Stoll, Phys. Rev. A **76**, 032507 (2007).
[58]J. Hoeft and K. P. R. Nair, J. Mol. Struct. **97**, 347 (1983).
[59]A. Borschevsky, V. Pershina, E. Eliav, and U. Kaldor, Phys. Rev. A **87**, 022502 (2013).
[60]W. W. Porterfield, *Inorganic Chemistry, A Unified Approach* (Academic Press, San Diego, 1993).
[61]D. R. Lide, *CRC Handbook of Chemistry and Physics*, 90th ed. (CRC, Boca Raton, FL, 2009-2010).
[62]W. Bacher and E. Jacob, in *Gmelin Handbuch der Anorganischen Chemie*, 8th ed., Uranium Supplement Vol. C8, edited by C. Keller and R. Keim (Springer-Verlag, Berlin, 1980).
[63]A. A. Maryott and F. Buckley, *Table of Dielectric Constants and Electric Dipole Moments of Substances in the Gaseous State, No 537* (U. S. National Bureau of Standards Circular, 1953).
[64]V. Pershina, J. Anton, and T. Jacob, J. Chem. Phys. **131**, 084713 (2009).
[65]M. Kamiya, H. Sekino, T. Tsuneda, and K. Hirao, J. Chem. Phys. **122**, 234111 (2005).
[66]J. T. H. Dunning, J. Chem. Phys. **90**, 1007 (1989).
[67]R. Kendall, J. T. H. Dunning, and R. Harrison, J. Chem. Phys. **96**, 6796 (1992).
[68]T. Noro, M. Sekiya, and T. Koga, Theor. Chem. Acc. **131**, 1124 (2012).
[69]K. G. Dyall, Theor. Chem. Acc. **108**, 335 (2002).
[70]K. G. Dyall, Theor. Chem. Acc. **117**, 483 (2007).
[71]K. G. Dyall, Theor. Chem. Acc. **112**, 403 (2004).
[72]K. G. Dyall, available from the Dirac web site http://dirac.chem.sdu.dk, 2016.
[73]K. G. Dyall, Theor. Chem. Acc. **99**, 366 (1998).
[74]A. Sadlej, Collect. Czech. Chem. Commun. **53**, 1995 (1988).
[75]A. Sadlej, Theor. Chim. Acta **79**, 123 (1991).
[76]A. Sadlej, Theor. Chim. Acta **81**, 45 (1991).
[77]A. Sadlej, Theor. Chim. Acta **81**, 339 (1992).
[78]V. Kellö and A. Sadlej, Theor. Chim. Acta **83**, 351 (1992).
[79]K. G. Dyall, Theor. Chem. Acc. **129**, 603 (2011).
[80]D. Woon and J. T. H. Dunning, J. Chem. Phys. **98**, 1358 (1993).
[81]Data base of Segmented Gaussian Basis Sets, Quantum Chemistry Group, Sapporo, Japan, 2014, http://setani.sci.hokudai.ac.jp/sapporo/Welcome.do.
[82]T. Noro, M. Sekiya, and T. Koga, Theor. Chem. Acc. **109**, 85 (2003).
[83]T. Noro, M. Sekiya, and T. Koga, Theor. Chem. Acc. **132**, 1363 (2013).
[84]N. Balabanov and K. Peterson, J. Chem. Phys. **123**, 064107 (2005).
[85]K. G. Dyall, J. Phys. Chem. A **113**, 12638 (2009).
[86]F. Weigend and R. Ahlrichs, Phys. Chem. Chem. Phys. **7**, 3297 (2005).
[87]D. A. Pantazis, X.-Y. Chen, C. R. Landis, and F. Neese, J. Chem. Theory Comput. **4**, 908 (2008).
[88]D. A. Pantazis and F. Neese, J. Chem. Theory Comput. **7**, 677 (2011).
[89]R. F. Barrow and R. M. Clement, Proc. R. Soc. A **322**, 243 (1971).
[90]K. P. R. Nair and J. Hoeft, J. Phys. B **17**, 735 (1984).
[91]L. C. Krisher and W. G. Norris, J. Chem. Phys. **44**, 391 (1966).
[92]K. P. R. Nair and J. Hoeft, Chem. Phys. Lett. **102**, 438 (1983).
[93]K. P. R. Nair and J. Hoeft, Phys. Rev. A **29**, 1889 (1984).
[94]T. C. Steimle, R. Zhang, and C. Qin, J. Phys. Chem. A **117**, 11737 (2013).
[95]T. Okabayashi, Y. Nakaoka, E. Yamazaki, and M. Tanimoto, Chem. Phys. Lett. **366**, 406 (2002).
[96]R. Zhang, T. C. Steimle, L. Cheng, and J. F. Stanton, Mol. Phys. **113**, 2073 (2015).
[97]C. Evans and M. Gerry, J. Mol. Spectrosc. **203**, 105 (2000).
[98]L. Reynard, C. Evans, and M. Gerry, J. Mol. Spectrosc. **205**, 344 (2001).
[99]F. V. Dijk and A. Dymanus, Chem. Phys. Lett. **5**, 387 (1979).
[100]K. P. Huber and G. Herzberg, *Molecular Spectra and Molecular Structure IV. Constants of Diatomic Molecules* (Van Nostrand Reinhold, New York, 1979).
[101]K. P. R. Nair, J. Hoeft, and E. Tiemann, Chem. Phys. Lett. **60**, 253 (1979).
[102]A. Durand, J. C. Loison, and J. Vigue, J. Chem. Phys. **106**, 477 (1997).
[103]E. Tiemann and A. Dreyer, Chem. Phys. **23**, 231 (1977).
[104]NIST Standard Reference Database Number 69, 2016, available at the following http://webbook.nist.gov/chemistry/.
[105]P. Schwerdtfeger, The ctcp table of experimental and calculated static dipole polarizabilities for the electronic ground states of the neutral elements, 2012, see http://ctcp.massey.ac.nz/dipole-polarizabilities and references cited therein.
[106]T. M. Miller and B. Bederson, Phys. Rev. A **14**, 1572 (1976).
[107]H. L. Schwartz, T. M. Miller, and B. Bederson, Phys. Rev. A **10**, 1924 (1974).
[108]C. Thierfelder, B. Assadollahzadeh, P. Schwerdtfeger, S. Schäfer, and R. Schäfer, Phys. Rev. A **78**, 052506 (2008).
[109]R. Bast, A. Heßelmann, P. Salek, T. Helgaker, and T. Saue, ChemPhysChem **9**, 445 (2008).
[110]V. Pershina, A. Borschevsky, E. Eliav, and U. Kaldor, J. Chem. Phys. **128**, 024707 (2008).
[111]C. Thierfelder and P. Schwerdtfeger, Phys. Rev. A **79**, 032512 (2009).
[112]U. Hohm and G. Maroulis, J. Chem. Phys. **124**, 124312 (2006).
[113]V. Pershina, A. Borschevsky, and M. Iliaš, J. Chem. Phys. **141**, 064314 (2014).
[114]B. Krebs and K.-D. Hasse, Acta Crystallogr., Sect. B: Struct. Crystallogr. Cryst. Chem. **32**, 1334 (1976).
[115]S. Díaz-Moreno and D. T. Bowron, Organometallics **22**, 390 (2003).
[116]V. Pershina, J. Anton, and T. Jacob, Phys. Rev. A **78**, 032518 (2008).
[117]G. Maroulis, Chem. Phys. Lett. **318**, 181 (2000).
[118]G. Maroulis, C. Makris, U. Hohm, and D. Goebel, J. Phys. Chem. A **101**, 953 (1997).
[119]L. Visscher and K. G. Dyall, J. Chem. Phys. **104**, 9040 (1996).